NAVAL POSTGRADUATE SCHOOL

MONTEREY, CALIFORNIA

THESIS

EVALUATION OF FRICTION STIR PROCESSING OF HY-80 STEEL UNDER WET AND DRY CONDITIONS

by

Garth William Young II

March 2012

Thesis Advisor: Terry McNelley
Second Reader: Sarath Menon

Approved for public release; distribution is unlimited

THIS PAGE INTENTIONALLY LEFT BLANK

REPORT DOCUMENTATION PAGE			Form Approved OMB No. 0704–0188
Public reporting burden for this collection of information is estimated to average 1 hour per response, including the time for reviewing instruction, searching existing data sources, gathering and maintaining the data needed, and completing and reviewing the collection of information. Send comments regarding this burden estimate or any other aspect of this collection of information, including suggestions for reducing this burden, to Washington headquarters Services, Directorate for Information Operations and Reports, 1215 Jefferson Davis Highway, Suite 1204, Arlington, VA 22202–4302, and to the Office of Management and Budget, Paperwork Reduction Project (0704–0188) Washington DC 20503.			
1. AGENCY USE ONLY *(Leave blank)*	**2. REPORT DATE** March 2012	**3. REPORT TYPE AND DATES COVERED** Master's Thesis	
4. TITLE AND SUBTITLE Evaluation of Friction Stir Processing of Hy-80 Steel Under Wet and Dry Conditions		**5. FUNDING NUMBERS**	
6. AUTHOR(S) Garth William Young II			
7. PERFORMING ORGANIZATION NAME(S) AND ADDRESS(ES) Naval Postgraduate School Monterey, CA 93943–5000		**8. PERFORMING ORGANIZATION REPORT NUMBER**	
9. SPONSORING /MONITORING AGENCY NAME(S) AND ADDRESS(ES) N/A		**10. SPONSORING/MONITORING AGENCY REPORT NUMBER**	
11. SUPPLEMENTARY NOTES The views expressed in this thesis are those of the author and do not reflect the official policy or position of the Department of Defense or the U.S. Government. IRB Protocol Number: N/A.			
12a. DISTRIBUTION / AVAILABILITY STATEMENT Approved for public release; distribution is unlimited		**12b. DISTRIBUTION CODE** A	

13. ABSTRACT (maximum 200 words)

This thesis describes the microstructural and mechanical property changes associated with Friction Stir Processing (FSP) of HY-80 steel under dry and underwater conditions. HY-80 is a low-carbon alloy steel that is used in a quenched and tempered condition and is highly susceptible to hydrogen assisted cracking associated with conventional fusion welding. FSW/P (400 RPM/ 2 IPM) was conducted using a polycrystalline cubic boron nitride tool having a pin length of 6.35 mm. Two sets of processing runs were completed on HY-80 plates, 6.35 mm in thickness, one dry and the other under seawater. Analysis of the residual hydrogen content revealed little change in hydrogen content associated with FSW/P. Detailed microstructural characterization (optical and scanning electron microscopy) with emphasis on the differences in the distribution of constituent phases in the rolling, transverse and normal planes was carried out. Microstructural analysis of the "plan-view" section at the tool extraction sites of FSW/P samples was executed. Mechanical properties of these samples were evaluated by tensile, microhardness, and Charpy V-notch impact resistance tests. The results indicated that austenitization occurred within the stir zones and subsequent cooling influenced the final microstructure and properties. The thermomechanically affected zone displayed a gradual change in near-equiaxed austenitic grain size towards both the tool axis as well as the base plate with little grain shape change throughout. These results have been rationalized on the basis of expected temperature and deformation fields generated setup in these steel samples and the nature of phase transformations occurring in low carbon steels such as HY-80.

14. SUBJECT TERMS Friction Stir Welding, Friction Stir Processing, Underwater Welding, High Strength Steel, Microstructural Properties, Hardenable Alloy Steel, Weld Repair, HY-80, Charpy Impact Test, Tensile Test, Microhardness Test, Martensite, Austenite			**15. NUMBER OF PAGES** 93
			16. PRICE CODE
17. SECURITY CLASSIFICATION OF REPORT Unclassified	**18. SECURITY CLASSIFICATION OF THIS PAGE** Unclassified	**19. SECURITY CLASSIFICATION OF ABSTRACT** Unclassified	**20. LIMITATION OF ABSTRACT** UU

NSN 7540–01–280–5500 Standard Form 298 (Rev. 2–89)
Prescribed by ANSI Std. 239–18

THIS PAGE INTENTIONALLY LEFT BLANK

Approved for public release; distribution is unlimited

EVALUATION OF FRICTION STIR PROCESSING OF HY-80 STEEL UNDER WET AND DRY CONDITIONS

Garth William Young II
Research Assistant, Naval Postgraduate School
B.S., California Polytechnic State University, 2009

Submitted in partial fulfillment of the
requirements for the degree of

MASTER OF SCIENCE IN MECHANICAL ENGINEERING

from the

NAVAL POSTGRADUATE SCHOOL
March 2012

Author: Garth William Young II

Approved by: Terry R. McNelley
Thesis Advisor

Sarath K. Menon
Second Reader

Knox T. Millsaps
Chair, Department of Mechanical and Aeronautical Engineering

THIS PAGE INTENTIONALLY LEFT BLANK

ABSTRACT

This thesis describes the microstructural and mechanical property changes associated with Friction Stir Processing (FSP) of HY-80 steel under dry and underwater conditions. HY-80 is a low-carbon alloy steel that is used in a quenched and tempered condition and is highly susceptible to hydrogen assisted cracking associated with conventional fusion welding. FSW/P (400 RPM and 2 IPM) was conducted using a polycrystalline cubic boron nitride tool having a pin length of 6.35 mm. Two sets of processing runs were completed on HY-80 plates, 6.35 mm in thickness, one dry and the other under seawater. Analysis of the residual hydrogen content revealed little change in hydrogen content associated with FSW/P. Detailed microstructural characterization (optical and scanning electron microscopy) with emphasis on the differences in the distribution of constituent phases in the rolling, transverse and normal planes was carried out. Microstructural analysis of the "plan-view" section at the tool extraction sites of FSW/P samples was executed. Mechanical properties of these samples were evaluated by tensile, microhardness, and Charpy V-notch impact resistance tests. The results indicated that austenitization occurred within the stir zones and subsequent cooling influenced the final microstructure and properties. The thermomechanically affected zone displayed a gradual change in near-equiaxed austenitic grain size towards both the tool axis as well as the base plate with little grain shape change throughout. These results have been rationalized on the basis of expected temperature and deformation fields generated setup in these steel samples and the nature of phase transformations occurring in low carbon steels such as HY-80.

THIS PAGE INTENTIONALLY LEFT BLANK

TABLE OF CONTENTS

LIST OF FIGURES

THIS PAGE INTENTIONALLY LEFT BLANK

LIST OF TABLES

THIS PAGE INTENTIONALLY LEFT BLANK

LIST OF ACRONYMS AND ABBREVIATIONS

BM – Base Material

BSD – Back Scatter Detector

CNC – Computer Numerical Controlled

EDS – Energy Dispersive Spectroscopy

FSP – Friction Stir Processing

FSW – Friction Stir Welding

FSW/P – Friction Stir Welding and/or Processing

GMAW – Gas Metal Fusion Welding

HAC – Hydrogen Assisted Cracking

HAZ – Heat Affected Zone

IPM – Inches per Minute

NPS – Naval Postgraduate School

PCBN – Polycrystalline Cubic Boron Nitride

PPM – Parts per Million

RPM – Rotations per Minute

SAW – Shielded Arc Welding

SEM – Scanning Electron Microscope

SDD – Silicon Drift Detector

SZ – Stir Zone

TMAZ – Thermo-Mechanically Affected Zone

USN – United States Navy

THIS PAGE INTENTIONALLY LEFT BLANK

ACKNOWLEDGMENTS

First, I would like to thank the Naval Postgraduate School for giving me an opportunity to become one of the few civilians to go through the Mechanical Engineering Program. Without this chance, I would have never been able to work such a unique kind environment with top researchers in the field.

A special thank you goes to Dr. McNelley for being my supervisor and thesis advisor, but as well for taking all my questions and being with me as I learned about FSW/P. He was someone who took a personal interest in my education and my professional career. It was under his field of expertise I was able to form my thesis.

Many thanks go to Dr. Sarath Menon for teaching me how to conduct research and how to become proficient in operating all the different instruments. I also thank him for always being available for guidance on both work and non-work related issues.

To MegaStir Technologies in Provo, Utah, thank you for conducting the friction stir welds and thank you to Murray W. Mahoney for providing your exemplary knowledge on friction stir technologies.

A very special thank you goes out to my wife, Rebekah Young. She understood the large amount of time and emotional commitment it takes while completing a thesis. I will always remember her staying up late to keep me company during the writing section.

Finally, thank you to my family and friends for always believing in me and pushing me to achieve my dreams.

THIS PAGE INTENTIONALLY LEFT BLANK

I. INTRODUCTION

The material of interest here, HY-80 steel, is high strength steel used in a quenched and tempered condition to achieve mechanical properties desired in many U.S. Navy applications, such as ship and submarine hulls, as well as some pressure vessels. This thesis will focus on the HY-80 used in the fabrication of the dive planes on nuclear submarines. Since the material is quenched and tempered, the resulting tempered martensitic microstructures confer the strengthening. However, this leaves the material susceptible to Hydrogen Assisted Cracking (HAC) as described by Masubuchi and Martin [1]. HAC happens when hydrogen diffuses into the material and concentrates at locations such as grain boundaries. This eventually leads to cracking. When conventional fusion welding is used on HY-80, there is a potential for hydrogen to be liberated from the water molecule and to diffuse/dissolve into the fusion zone. Hydrogen diffusion in weld metal cannot be prevented; however, extensive site preparation and strict environmental controls can be used to restrict the amount of diffusible and residual hydrogen in the resulting weldment. The material preparation requires pre- and post-heating of the materials to be welded, filler electrode controls such as baking and storing and control of moisture and hydrocarbons. Due to these strict environmental controls, performing conventional fusion welding underwater would require expensive site preparation and, likely, prolonged repair time according to “Underwater repair technology” by Nixon [2].

In the United States Navy, Los Angeles-class submarines have been found to develop dive plane cracks due to the stresses of changing depth. When found, cracks are noted and scheduled for repair during the next dry docking interval. The repair of the dive planes may entail drilling holes in the dive planes to thoroughly drain out any water and placing of heating blankets. The cracks and these holes are then repaired with conventional fusion welding. This process has the potential to extend the stay in dry dock if problems arise or due to the aforementioned extensive site preparation and strict environmental controls.

An alternative to conventional fusion welding is friction stir welding (FSW) and friction stir processing (FSP). FSP and FSW are solid state processes for the joining and processing of different materials. Friction stir welding/processing (FSW/P) were invented by The Welding Institute in Cambridge, United Kingdom in 1991 [3]. FSW/P has been implemented into the U.S. Navy in such applications as joining aluminum material on Littoral Combat Ships along with the surface treatment of nickel aluminum bronze propellers. In the last ten years, research on FSW/P of steels has received increasing attention.

The process of friction stirring involves a cylindrical tool with a shoulder and a projecting pin. The tool is spun at pre-determined revolutions per minute (RPM) and then plunged into the material and traversed across it. Friction stir processing can be done on a single sheet of material to change the mechanical properties by changing the microstructure. For friction stir welding, plates can be abutted and joined by traversing the tool along the seam line. An anvil is placed under the material to react the plunge force. As the tool traverses along the weld line, the material undergoes severe plastic deformation under adiabatic conditions and is simultaneously heated via frictional and adiabatic dissipation. Figure 1 illustrates the basic FSW/P nomenclature.

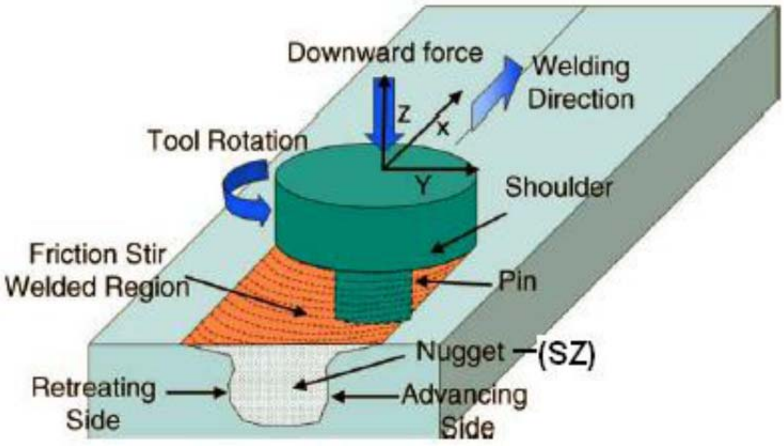

Figure 1. FSW/P Nomenclature [From 4].

This thesis continues and builds upon prior work conducted by Norman Overfield [5] and William Stewart [6]. Overfield demonstrated that FSW/P can be performed on a hardenable alloy steel (AISI 4142) in dry ambient conditions and also underwater. He also concluded that the hydrogen concentration in FSW/P material for both dry and underwater conditions was well within acceptable levels for high-strength steels. Stewart conducted initial experimentation on FSW/P of HY-80 or 100 both in dry and wet conditions. This thesis verifies that FSW/P can be successfully conducted on HY-80 under both a dry ambient condition and underwater while minimizing defects and re-distributing inclusions, along with producing acceptable hydrogen content.

THIS PAGE INTENTIONALLY LEFT BLANK

II. BACKGROUND

Friction Stir Welding (FSW) has been used primarily for joining of low melting metals such as Aluminum and Magnesium alloys. Peak process temperatures are typically 450–500 °C, and conventional tool steels have adequate wear resistance to withstand such operating conditions. However, the application of FSW to steels and other higher melting temperature materials has been limited by the lack of suitable tool materials, since operating temperatures higher than 1000 °C are necessary in order to achieve adequate deformation of the materials to be joined [7].

In recent years, there has been an increase in potential tool materials. DP980 (advanced high-strength steel) [8] and SKD61 tool steel [9] have been examined. However, for steels, polycrystalline cubic boron nitride (PCBN) is the most suitable tool material and was used in this work. PCBN is typically used as an abrasive and is most commonly used as a tool material for iron, nickel and other alloys at high temperature. When PCBN comes in contact with oxygen at high temperatures, a passivation layer of boron oxide forms on the surface and protects the material from further deterioration. [10]

After FSW/P, the resulting microstructures are highly dependent upon the chemical composition of the base material as well as the weld parameters; revolutions per minute (RPM), inches per minute (IPM), and plunge force. Parameters ranging from 1000 RPM/ 15 mm/s (35 IPM) [11] to 100 RPM 25 mm/min (1 IPM) [12] have been shown to produce defect-free welds. Recorded plunge force can range from 5 kN (1125 lbf) to 40 kN (8900 lbf) [13]. According to Overfield [3], the best combinations of RPM and IPM for steels were 400 and 2, respectively. This was shown to produce a homogenous and defect-free weld. The plunge force is typically set at a constant known parameter that produces an even weld depth, minimizing the flash. Variable plunge force can be set to compensate with any unexpected changes in material height or surface anomalies.

In friction stir processed steels, a martensitic microstructure is commonly produced in the stir zone and the thermomechanically affected zone (TMAZ) [7, 14]. This indicates that the peak temperature in the stir zone is in the austenite range for the material. After rapid cooling, the prior austenite grains become untempered martensite. However, one study was conducted on high strength steel in which the welding parameters and cooling rates were controlled to produce a martensite-free weld by not allowing the temperature in the SZ to not exceed the A_1 temperature [14]. This study shows that by controlling the cooling curves, the microstructure can be controlled and therefore the material can be processed to possess different mechanical properties [7, 14].

The only known studies of FSW/P of steel being conducted underwater are those reported by Overfield [3] and Stewart [4]. FSW/P conducted underwater on steels has the potential to replace conventional fusion welding. Underwater fusion welding requires extensive site preparation and strict environmental controls. There is a higher potential for HAC due to the high temperature of the arc under the water. The energy from the arc tends to dissociate the water molecule to produce large amounts of monoatomic hydrogen which then will diffuse into the weld. There are no industry standards to weld HY-80 underwater [15].

HY-80 is a low carbon alloy steel that acquires its strength and toughness through quenching and tempering. HY-80 has an upper limit of 0.18 wt% carbon. Nickel and chromium are used to reduce the ductile-brittle transition temperature and enhance the hardenability. The sulfur and phosphorous contents are strictly controlled so they do not exceed 0.045 wt% together [16]. The composition limits can be seen in Table 1. HY-80 is made by either the open hearth or the electric furnace process. The resulting steel is fully killed and fine grained. Plates are then rolled directly from either ingots or slabs. A final heat treatment of quenching and tempering is conducted to achieve the desired strength and toughness. Due to this final heat treatment, the steel is susceptible to hydrogen assisted cracking which conventional fusion welding can contribute. The phase diagram of Fe-C shows the phases that are produced when performing conventional

fusion welding and that of FSW/P, Figure 2. This thesis will compare the hydrogen content between base metal, conventional fusion welding, and FSW/P to determine if FSW/P will also contribute to HAC.

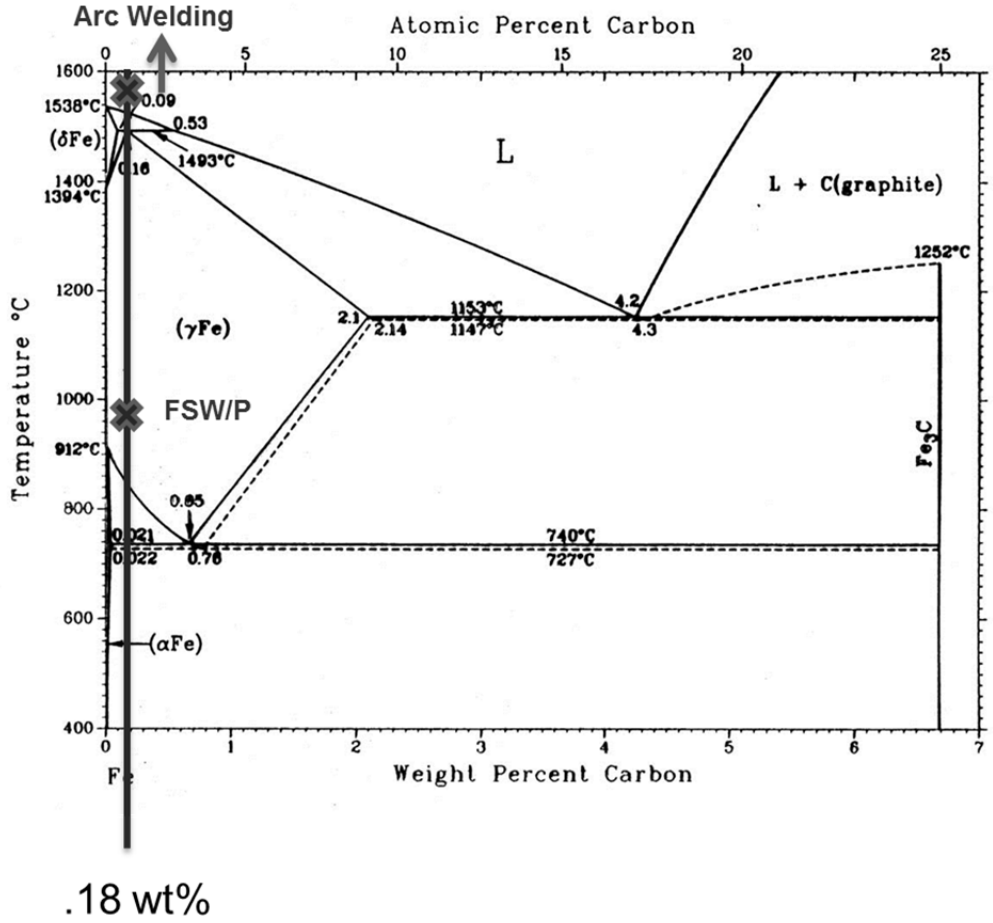

Figure 2. Fe-C phase diagram showing the temperature regime for fusion welding and FSW/P.

Overfield [3] concluded that FSW/P can be conducted on AISI 4142 grade steel in both a dry ambient condition as well as underwater. He also concluded that the best weld parameters for FSW/P of steel was a RPM of 400 and an IPM of 2, which would produce defect free welds. A comparison of the hydrogen content from the base material to that of FSW/P material showed that the hydrogen content was within the acceptable limits.

Stewart [4] conducted a preliminary analysis of the base material of HY-80 and compared it to that of FSW/P. He concluded that FSW/P could be done in an ambient dry condition along with underwater. He also indicated that the microstructure of the base material was tempered martensite and an untempered martensite in the FSW/P stir zone.

III. EXPERIMENTAL PROCEDURE

A. HY-80 MATERIAL

1. Acquisition

A plate of HY-80 steel was obtained from Naval Surface Warfare Center, Carderock Division, Bethesda, MD. The dimensions of the plate were 43.5 inches (110.5 cm) long, 26.5 inches (67.3 cm) wide, and 0.25 inches (6.4 mm) thick. The rolling and transverse directions of the plate were identified and carefully noted during the characterization of the properties and microstructural variation with respect to the plate and processing conditions.

2. Plate Chemistry

A 1.0 inch (25.4 mm) by 1.0 inch (25.4 mm) by 0.25 inch (6.4 mm) sample was sectioned from a corner of the plate using a Struers Sectom-10 diamond saw. This sample was sent for chemical analysis at Anamet, Inc., Hayward, CA, to determine the chemical composition of the steel used in this work. Table 1 gives the composition limits for HY-80 steel according to MIL-S-16216K [16].

Element	**Min (wt%)**	**Max (wt%)**
Carbon (C)	0.12	0.18
Chromium (Cr)	1.00	1.8
Copper (Cu)	---	0.25
Manganese (Mn)	0.10	0.40
Molybdenum (Mo)	0.20	0.60
Nickel (Ni)	2.00	3.25
Phosphorous (P)	---	0.025*
Silicon (Si)	0.15	0.35
Sulfer (S)	---	0.025*
Titanium (Ti)	---	0.02
Vanadium (V)	---	0.03
* P + S = 0.045 MAX		

Table 1. Chemical composition limits for HY-80 (in wt %).

3. Sectioning

The large plate was sectioned into 3 smaller plates: A, B and C. The 3 plates had the dimensions of 26.5 inches (67.3 cm) by 14.5 inches (36.90 cm). The thickness remained 0.25 inches (6.4 mm). Plate A was friction stir processed, plate B was studied for base material mechanical properties and metallographic analysis, and plate C was retained for future work. The surface was sand blasted to remove any loosely adherent oxides prior to friction stir processing.

B. FRICTION STIR PROCCESSING

1. Sample Preparation

Plate A was sand blasted and then surface ground to remove the mill-scale. Plate B received similar treatment. Then, plate A was further sectioned to provide two 26.5 inch (67.3 cm) by 7.25 inch (18.45 cm) plates, A_1 and A_2. The A_1 plate received dry friction stir processing and plate A_2 was subjected to underwater friction stir processing. Both HY-80 sections were provided to MegaStir Technologies in Provo, Utah.

2. Friction Stir Processing

Plates A_1 and A_2 were clamped to the worktable of a converted K&T milling machine, Figure 3. The MegaStir FSW/P mill has a low run-out spindle specifically designed to withstand the forces needed to produce friction stir welds on ferrous alloys. The K&T mill was capable of both position and force control.

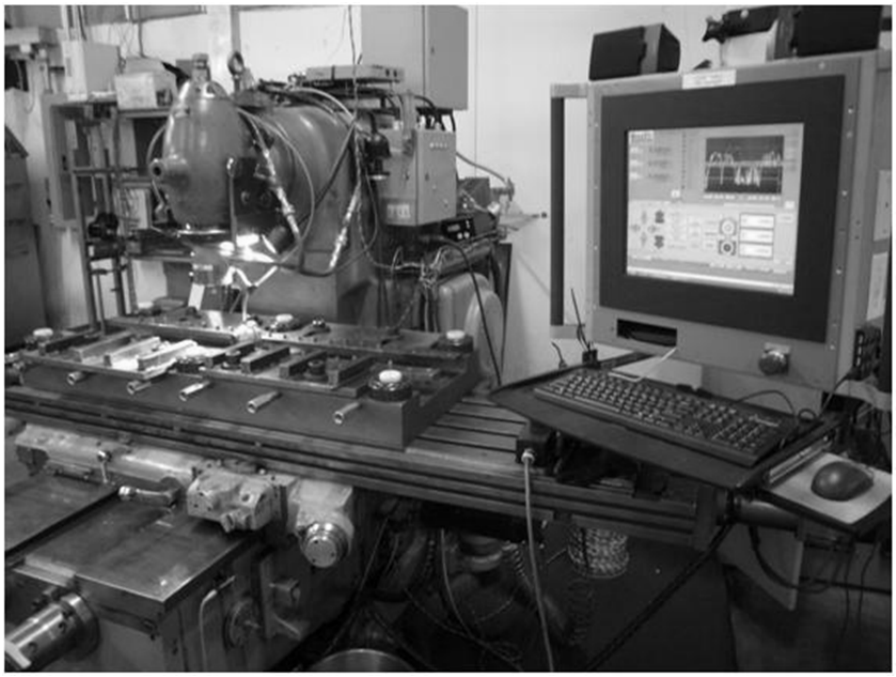

Figure 3. MegaStir K&T FSW milling machine.

The tool used to conduct both underwater and dry friction stir processing was polycrystalline cubic boron nitride (PCBN) embedded in a tungsten-rhenium (W-Re) binder, Figure 4. The tool material is also designated as MS80. The tool design included a convex scroll shoulder with a step-spiral protruding pin (CS4).

Figure 4. PCBN FSW/P threaded tool.

For the dry friction stir weld a 25 inch (63.5 cm) weld was conducted in the direction transverse to the rolling direction, Figure 5. The FSW/P was conducted at 400 RPM and a travel speed of 2 IPM. These conditions were based on a previous study conducted on AISI 4142 steel by Overfield [3]. A plunge force of 15,000 pounds was applied and then decreased to 10,000 pounds after the pin was fully inserted. Due to a computer error during the run, the tool was extracted after a short distance. The tool was reinserted and the processing continued normally for another 12 inches (30.5 cm). However, surface flaws appeared on the advancing side of the tool towards the end of the run, Figure 6. This could have been due to poor surface finishing of the HY-80. It also appeared to create a tunneling defect that ran a short distance along the weld. Due to these flaws, a second dry FSW/P run was conducted along a line offset from the previous run after cleaning the surface further with grinding. This seemed not to decrease the defects but did reduce the weld flash.

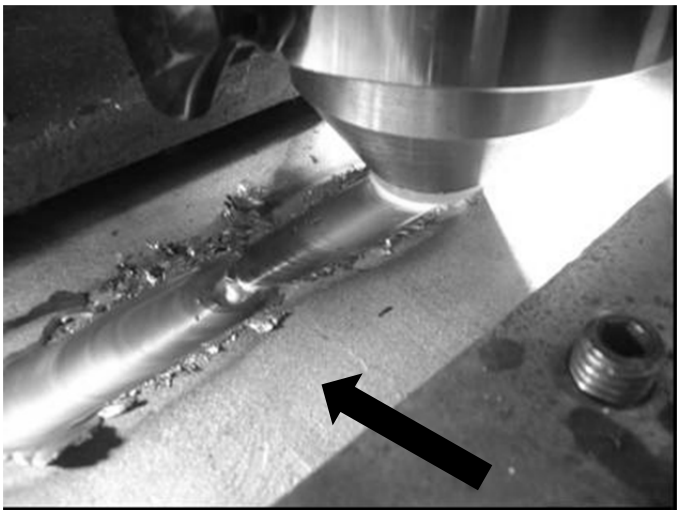

Figure 5. Dry FSW/P in-progress showing a second plunge after a computer failure extraction.

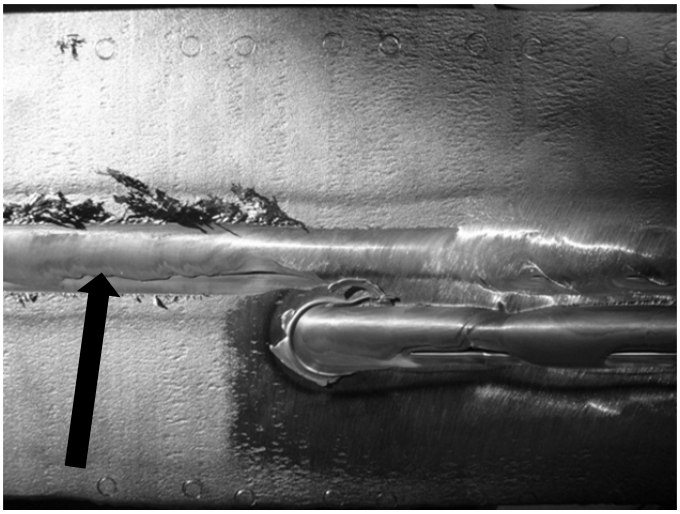

Figure 6. Surface flaws on advancing side during dry FSW/P and second dry FSW/P offset.

In order to conduct underwater FSW/P, a special apparatus was created to adhere to the top of the steel plate with silicon glue. A clear Plexiglas box 4 inches (101.6 mm) high was constructed for this purpose. In order to create an environment similar to the ocean and to inhibit water boiling, a copper pipe attached to a chiller was inserted through the Plexiglas box and cooling water was pumped through during the FSW/P process, Figure 7. Sea salt was added to distilled water to create a 3.5% salt content.

Figure 7. HY-80 plate attached to Plexiglas chamber with copper piping for underwater FSW/P.

Two separate underwater runs were conducted because of the size limitations of the underwater chamber. Each run was approximately 10 inches (25.4 cm). This produced a total of 20 inches (50.8 cm) of underwater friction stirred HY-80.

The same parameters were used for underwater FSW/P as those used in dry FSW/P, 400 RPM and 2 IPM. Figure 8 shows underwater FSW/P in progress. The plunge force was higher at 17,000 pounds and was reduced to 10,000 pounds during the equilibrium weld section. At the end, there was a little weld flash but there were no visible weld defects, Figure 9. The water was drained and the box was moved over in order to conduct the second underwater FSW/P. However, during the second run, there was a leak at the box/plate intersection, and water drained out. Tap water was added during the weld to keep the tool and material submerged throughout the entire process.

Figure 8. Underwater Friction Stir Welding of HY-80.

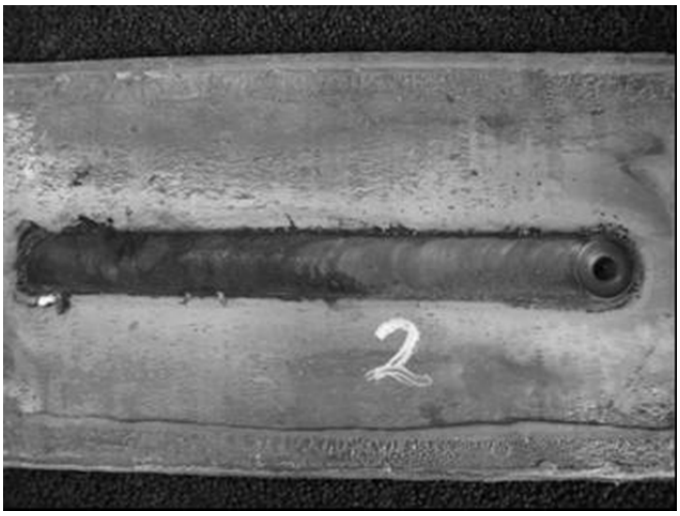

Figure 9. Surface Appearance of Underwater FSW/P.

C. CHEMICAL TESTING

To determine the levels of hydrogen that were absorbed from the friction stir process, samples 1.0 inch (25.4 mm) by 0.25 inch (6.4 mm) from the weld zones were sectioned and sent to Luvak Inc., Boylston, MA. Vacuum hot extraction was used to determine the hydrogen concentration as specified by ASTM E 146–83. In addition, combustion infrared detection and direct current plasma emission spectroscopy were used to determine the amounts of other alloying elements.

D. IMPACT ENERGY TESTING

1. Sample Geometry

From the HY-80 plates, approximately 32 inches (81.3 cm) of usable, defect-free friction stir processed material was obtained in both the wet and dry conditions. The goal was to produce as many Charpy impact energy samples as possible while also obtaining tensile samples for the two conditions. Figure 10 shows the layout and orientation of the test samples on the HY-80 plates. Charpy and tensile samples were also obtained from plate C (base material). A total of 187 Charpy impact samples were machined from base material; 29 samples from underwater FSW/P, 24 samples from the dry run plate, two tensile samples from the underwater FSW/P and two tensile samples from the dry FSW/P. From the base material, four tensile samples were machined parallel to the rolling direction and five tensile samples oriented in the transverse direction.

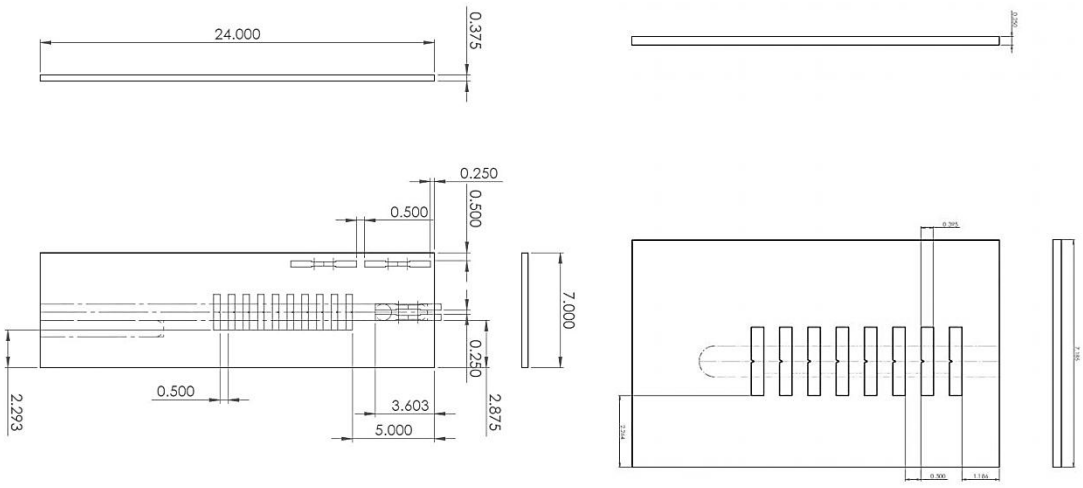

Figure 10. Machining layout dry FSW/P on left, underwater FSW/P on right.

All Charpy V-Notch samples were machined following ASTM Standard E23–07a, Figure 11. These Charpy samples were sub-sized specimens with the cross section of 5 mm X 10 mm. They were first cut out using a band saw and then milled down to above specification using a CNC mill.

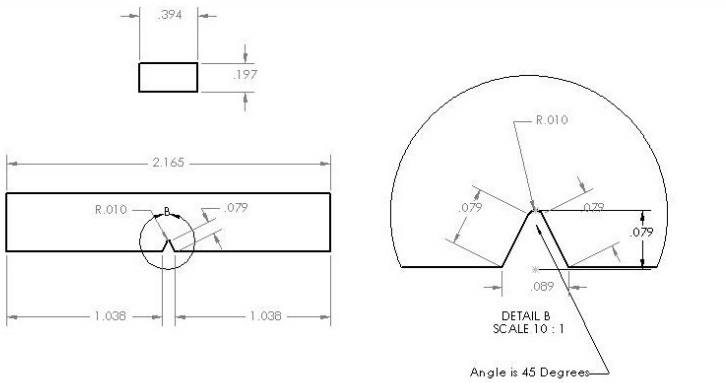

Figure 11. Charpy V-Notch sample, ASTM Standard E23–07a.

2. Sample Orientation

Charpy impact energy depends on morphology of inclusions which are generally elongated in the hot rolling direction, and sample orientation plays an important role in the mechanical properties. In order to obtain Charpy impact resistance values of HY-80 in relation to the rolling direction, samples were machined in both directions to produce a more comprehensive understanding of how the material behaves. When the elongated inclusions lie in the plane of fracture, the Charpy impact energy is expected to be low, while higher Charpy impact energy will be observed when inclusions lie orthogonal to crack propagation. On the base material, samples were cut with the crack propagation direction in both the transverse and longitudinal direction in relation to the rolling direction, Figure 12.

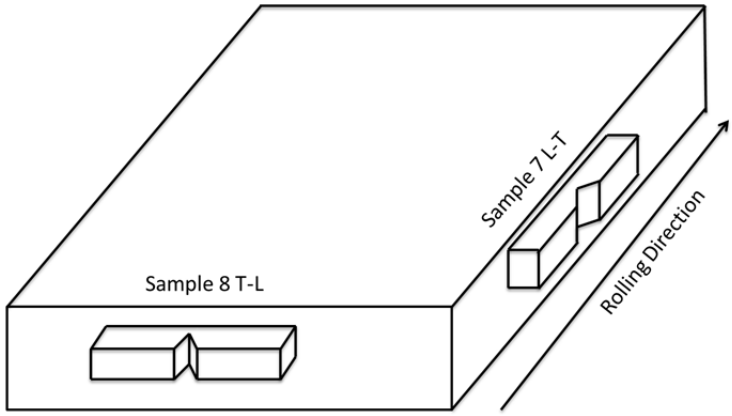

Figure 12. Charpy V-Notch base material sample orientation.

For both the dry and underwater FSW/P, the Charpy V-Notch samples were machined with the direction of the crack propagation in parallel to FSW/P tool direction, with the notch aligned in the direction the tool was traveling.

3. Test Procedure

Three each Charpy V-Notch samples were chilled for five minutes at a variety of temperatures shown in Table 2. Temperatures were obtained by mixing ice, salt, water, liquid nitrogen, and ethanol together in varying amounts in an insulated container. Samples were quickly transferred from baths to Charpy Impact Energy tester and broken. Samples were removed and washed with methanol to preserve the fracture surface for future fractography examination.

Base Material		**Wet and Dry FSW/P Samples**	
°C	Solution	°C	Solution
20.5	Room Temp	20.5	Room Temp
-10	Ice and Salt Water (NaCl)	0	Ice and Salt Water (NaCl)
-28	Ethanol and Ice	-50	Ethanol and LN_2
-48	Ethanol and LN_2	-90	Ethanol and LN_2
-60	Ethanol and LN_2	-110	Ethanol and LN_2
-70	Ethanol and LN_2	-200	LN_2
-90	Ethanol and LN_2		
-120	Ethanol and LN_2		

Table 2. Test temperatures of Charpy V-Notch samples.

E. TENSION TESTING

1. Sample Geometry

Base material, dry FSW/P, and underwater FSW/P tensile samples were machined using a band saw and CNC controlled mill. ASTM E8/E8M-08 specimen geometry was used as shown in Figure 13.

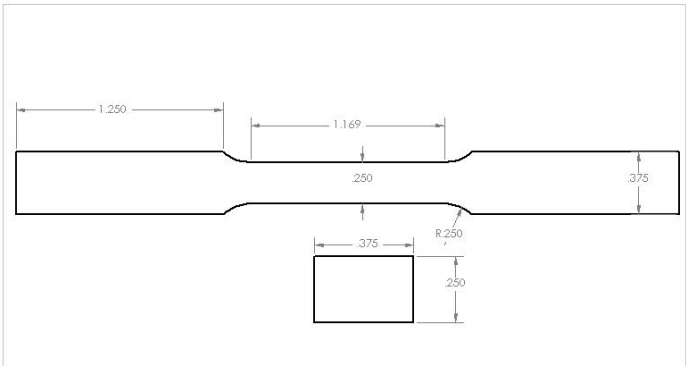

Figure 13. Tensile test sample, ASTM E8/E8M-08.

2. Sample Orientation

Base material samples were machined in two different directions: parallel to the rolling direction and the transverse direction. The dry FSW/P tension samples were machined so that the gauge length was parallel to the weld direction. The underwater FSW/P tension samples were machined the same way as dry FSW/P.

3. Test Procedure

Tensile testing was conducted using an Instron tensile test machine. Tensile testing was performed on two dry FSW/P samples, two underwater FSW/P directions, five transverse to the rolling direction base material samples, and five base material samples parallel to the rolling direction. All tension samples were conducted using a strain rate of 2.1 x 10^{-3} per second.

F. METALLOGRAPHIC TECHNIQUES

1. Sectioning and Mounting

The morphology of the inclusions was observed by examining metallographically polished sections that were parallel to the fracture surface as well as perpendicular to it. Each sample was sectioned into two different orientations using a Struers Sectcon-10 saw fitted with an Al_2O_3 cutting disc. The two directions for each sample were transverse to the inclusions and parallel to the elongated inclusions as indicated in Figure 14.

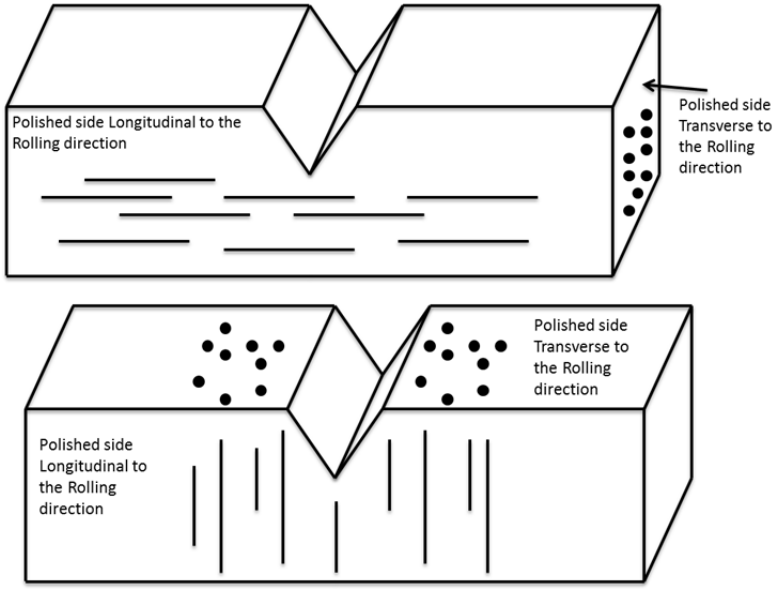

Figure 14. The orientation of the metallographically polished surfaces are illustrated in this schematic diagram (Top) Transverse to the rolling direction (L-T) polishing surfaces (Bottom) Longitudinal to the rolling direction (T-L) polishing surfaces.

All base material samples for metallographic preparation were mounted using a hot mount Bakelite powder that was heated and pressurized in a Buehler Hot Mount Press. Figure 15 shows the two orientations for each sample mounted in a puck. This allowed for easier grinding, polishing, and the ability to use Buehler AutoMet 2 multi-sample Grinder/Polisher.

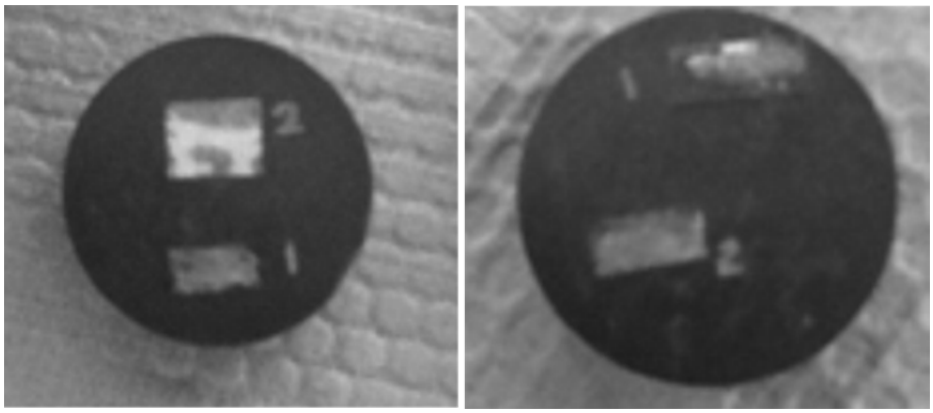

Figure 15. Hot mounted metallographic samples.

Charpy V-Notch tested samples were used for metallographic examination for both the dry and underwater FSW/P runs. The samples were mounted in a cold mount epoxy using Buehler Sample Kwick Liquid and Powder.

The “plan view” of the pin extraction site was examined to determine characteristics of temperature and deformation fields around the FSW/P tool. The extraction site was examined by sectioning the plate and then orientating it in a way to advancing edge. In Figure 16, the bold black square represents the metallographically prepared sample. These sections were mounted using the Buehler Kwick cold mounting supplies.

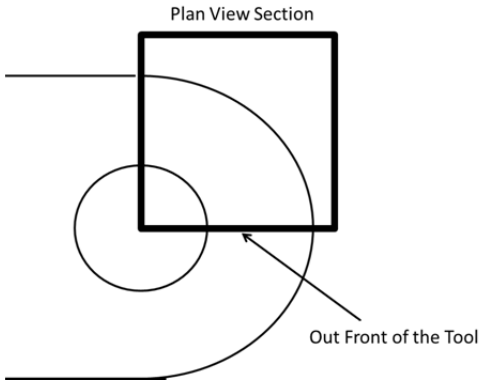

Figure 16. Schematic of sectioning of pin extraction zone with FSW/P direction to the right.

2. Grinding

Grinding for all samples followed the same procedure and used same supplies. Grinding began with 120P grit Al_2O_3 paper and worked through 220P, 500P, 1500P grit grinding paper. Samples were ground on each paper for approximately thirty minutes with 5–10 lbs. of variable force. Samples were ground by hand and using Buehler Ecomet 4 polisher and Automet 2 multi sample polisher.

3. Polishing and Etching

Polishing for all samples followed the same procedure and used the same supplies. Polishing began with 5 µm Al_2O_3 suspended in tap water on Buehler 8” Microcloth and on through 3 µm and 1 µm suspensions. Samples were polished with

each Al_2O_3 suspension for approximately 30 minutes with 5–10 lbs. of variable force. Samples were polished by hand and using a Buehler Ecomet 4 polisher and Automet 2 Multi-sample polisher. Final polishing for all samples was conducted using a .5 µm Al_2O_3 suspension for an hour by hand.

All prepared samples were etched using a 5% Nital etchant (5% HNO_3 and 95% Ethanol). After five seconds of emersion in the etchant, samples were rinsed off thoroughly with tap water, sprayed with Methanol, and dried with a heat gun.

G. OPTICAL MICROSCOPY

Optical microscopy was conducted on each polished sample using a Nikon Epiphot 200 equipped with NIS-Elements software. Montages and higher resolution images were taken at 25x, 100x, 200x, 500x, and 1000x magnification. Locations of interest were the base material orientations, thermomechanically affected zone, and stir zone. The 25x magnification micrographs were combined to make a montage of the material using Adobe Photoshop CS.

H. SCANNING ELECTRON MICROSCOPY

1. Sample Preparation

Mounted samples were removed from their cold/hot mounts without damaging the polished surface by using a vice to break the epoxy. Samples were bonded to a metal stage to disperse the electron build up and charging during examination in the SEM. This was achieved with either silver paste or carbon tape.

Fractured samples were preserved by rinsing with methanol, drying and placing them in a vacuum desiccator immediately after they were broken by either impact energy testing or tensile testing.

2. High Resolution Imaging

High resolution imaging was conducted using the Naval Postgraduate School's Zeiss Neon 40 scanning electron microscope that is equipped with field emission filament. However, half-way through the study the Zeiss SEM had a mechanical failure and the samples were further analyzed using Naval Postgraduate Schools (NPS) Topcon

SM-510 SEM with a LaB_6 filament, Figure 17. Both microscopes imaged the samples at an accelerating voltage of 15 KeV or 20 KeV with a working distance of around 5 mm (Zeizz) or 22 mm (TOPCON).

Figure 17. (Left) FESEM Zeiss Neon 40 (Right) TOPCON SM-510.

3. Energy Dispersive Spectroscopy (EDS)

EDS was conducted on base material and FSW/P runs to determine compositional data and qualitative data on inclusion stringers. The EDAX system on the Zeiss uses a Silicon Drift Detector (SDD) and the EDS on the TOPCON uses a Silicon Lithium (SiLi) detector aided by a 10 L Liquid Nitrogen tank for cooling.

I. MICROHARDNESS TESTING

Microhardness measurements were conducted using a HVS-1000 digital microhardness tester. A test load of 9.8 N with a 15 sec dwell time was used with a loading and unloading rate of 20 N/min. Microhardness data was taken on base material at random locations to provide an average microhardness. Microhardness was taken on both dry and underwater FSW/P pin extraction zones on the leading edge of the tool advancement direction at intermediate steps of 0.05 mm. Multiple microhardness

traverses at varying depths were conducted on dry and wet FSW/P samples transverse to the direction of FSW/P tool travel. Figure 18 illustrates the placement of microhardess sites with respect to depth.

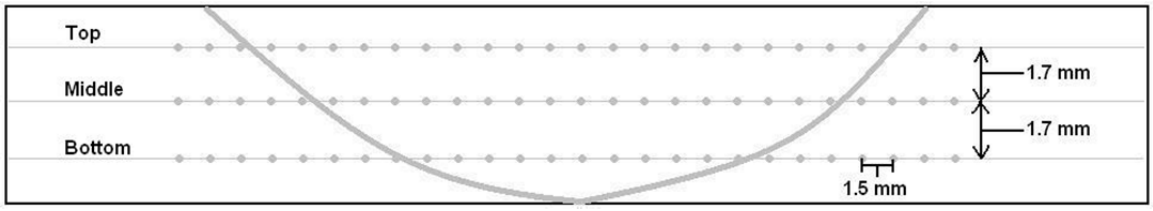

Figure 18. Illustration of placement of microhardness points in relationship to depth.

IV. RESULTS AND DISCUSSION

A. VISUAL INSPECTION

The as-received plate was cleaned by sand blasting. Due to the surface groves and defects on the base material the prior rolling direction was made apparent.

After the dry friction stir process, there were surface defects: flash developed on the sides due to the tool placement being too deep and a visual tunneling defect as shown in Figure 19. The flash is due to excessive plunge force that was controlled by computer numerical control (CNC), and which was corrected in the wet FSW/P.

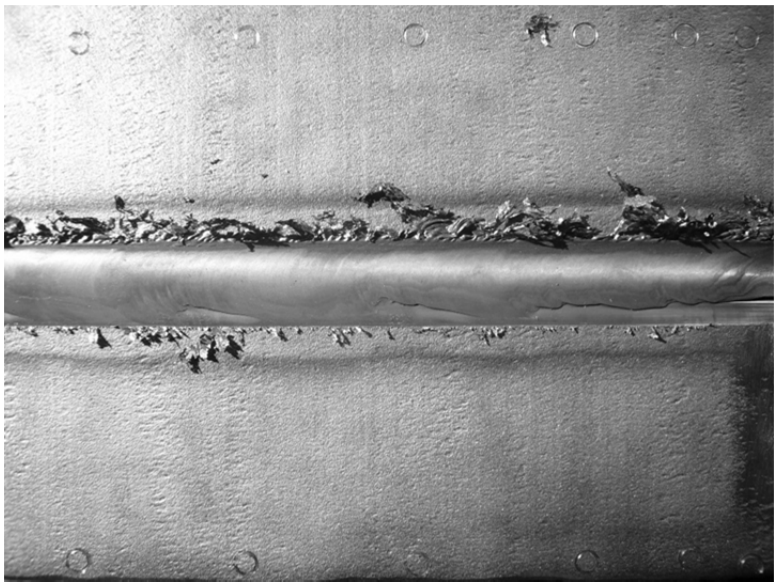

Figure 19. Dry FSW/P demonstrating flash from excessive plunge force.

The underwater FSW/P demonstrated evidence that weld parameters were improved due to the observation of less surface defects, minute weld flash, and no visual sign of tunneling defects on the surface, Figure 20. This was achieved by manually operating the downward force to keep the shoulder of the tool flush with the surface of the plate.

The underwater FSW/P weld exhibited distinct signs of corrosion. This was presumably caused by the freshly exposed HY-80 coming in contact with salt water, and also the aforementioned normal oxidation of a low carbon steel.

Figure 20. Underwater FSW/P demonstrating absence of tunneling defect.

On all plates, there was full penetration for the weld depth. This was observed by inspecting the underside of the plates and detecting discoloration. However, in the underwater FSW/P there was a hole observed indicating that the depth of the tool was too deep, Figure 21.

Figure 21. Full weld penetration of the underside of the underwater FSW/P plate.

B. CHEMICAL ANALYSIS

1. Base Metal Composition

Chemical testing conducted at Luvak Inc and Anamet concluded that the base material was within the compositional requirements of HY-80 specified in MIL-S-16216K (SH) [16]. Table 3 includes the measured and required chemical composition of the HY-80.

Element	Min (wt%)	Max (wt%)	Luvak*	Anamet**
Carbon (C)	---	0.18	.17	0.167
Chromium (Cr)	1.00	1.8	1.59	1.52
Copper (Cu)	---	0.25	0.23	0.09
Manganese (Mn)	0.10	0.40	.38	0.39
Molybdenum (Mo)	0.20	0.60	0.27	0.24
Nickel (Ni)	2.00	3.25	2.29	2.33
Phosphorous (P)	---	0.025*	0.009	0.015
Silicon (Si)	0.15	0.35	0.25	0.24
Sulfer (S)	---	0.025*	0.028	0.015
Titanium (Ti)	---	0.02	<0.005	<0.005
Vanadium (V)	---	0.03	0.008	0.01
* P + S = 0.045 MAX				

Table 3. Measured and required chemical composition of HY-80 steel.

2. Hydrogen Content

High strength steels are susceptible to hydrogen assisted cracking. FSW/P does not involve a high enough temperature to significantly dissociate the water molecule and liberate hydrogen. To be able to implement friction stir welding, the hydrogen content

must be less than the hydrogen content due to conventional welding or within acceptable limits. This will be an important factor for the FSW/P runs completed underwater.

According to MIL-H-6875 for shielded arc welding, the range of allowable hydrogen values in a deposited weld is 2.0 to 5.5 ml H_2/100 g metal [17]. This is included in Table 4 in the columns labeled GMAW and SAW. The goal was to limit the maximum permissible hydrogen to less than that of conventional welding.

The results of the vacuum hot extraction hydrogen testing showed that the hydrogen content in the material increased marginally in the underwater friction stir process and decreased in the dry friction stir process as shown in Table 4. In both dry and wet FSW/P, it is important to note that the hydrogen content of the stir zone is within acceptable ranges. The hydrogen content probably decreases in the dry FSW/P due to the material being heated and the escape of hydrogen into the atmosphere. From Table 4, it appears that the hydrogen content of the underwater FSW/P is 20% higher than the base material. However, the error in the vacuum hot extraction process is around 5 to 10%, and it is difficult to conclude that the increased hydrogen content in the underwater FSW/P is due to the production of atomic hydrogen (by dissociation). The GMAW and the SAW referenced in Table 4 were all conducted according to MIL-STD-248 [18]

	FSW/P			GMAW	SAW
	Base	Wet	Dry	Base	Base
	ml/100g	ml/100g	ml/100g	ml/100g	ml/100g
Hydrogen	2.13	2.58	1.01	2.0–5.0	3.0–5.5

Table 4. Comparison of diffusible Hydrogen (ppm) in BM, Wet and Dry FSW/P to Fusion Welding [After 17].

The Luvak Inc. results were reported in ppm and where converted to ml/100 g using the 1.0 ml H_2/100 g metal at STP = 0.89 ppm hydrogen in steel [19]. Compared to conventional fusion welding, the residual hydrogen is significantly less in the friction stir processed material. This means that there is less opportunity for hydrogen assisted cracking to occur.

In both dry and underwater FSW/P, the hydrogen content was below the allowable range or in the lower end of this range for conventional fusion welding processes and supports the contention that FSW/P is a viable means to produce welds with low hydrogen content. There was no pre- or post-weld heat treatment and no shielding gases were used during the FSW/P welds. There have been studies where engineers have added the use of a shielding gas in the application of FSW/P to further protect the heated metal from atmospheric contamination [6, 9, 11, 13, 15, 20].

A study on FSW/P aluminum hypothesizes that an increase in hydrogen content in underwater FSW/P is due to the chemical reaction of the water with the freshly exposed metal [21]. This freshly exposed aluminum surface undergoes an oxidation reaction with water, resulting in the liberation of H/H_2. According to these authors, the hydrogen content is not directly related to the high temperature being generated from the FSW/P tool but instead the result of the chemical reaction. Further research is required to apply this theory to steels.

C. METALLOGRAPHY

1. Optical

a. Base Material

As mentioned in the background section, HY-80 is a hot rolled material with distinct rolling and transverse directions. Observing the un-etched material, many inclusions and defects can easily be seen, Figure 22. From the etched micrographs a tempered martensitic microstructure was found comparable to that in similar steels, Figure 23. Dark bands in the rolling direction are due to the inclusion stringers.

Figure 22. Montage of low magnification micrographs from base material displaying band-like distribution caused by hot rolling (rolling direction from left to right. Notice long elongated inclusions in the rolling direction.

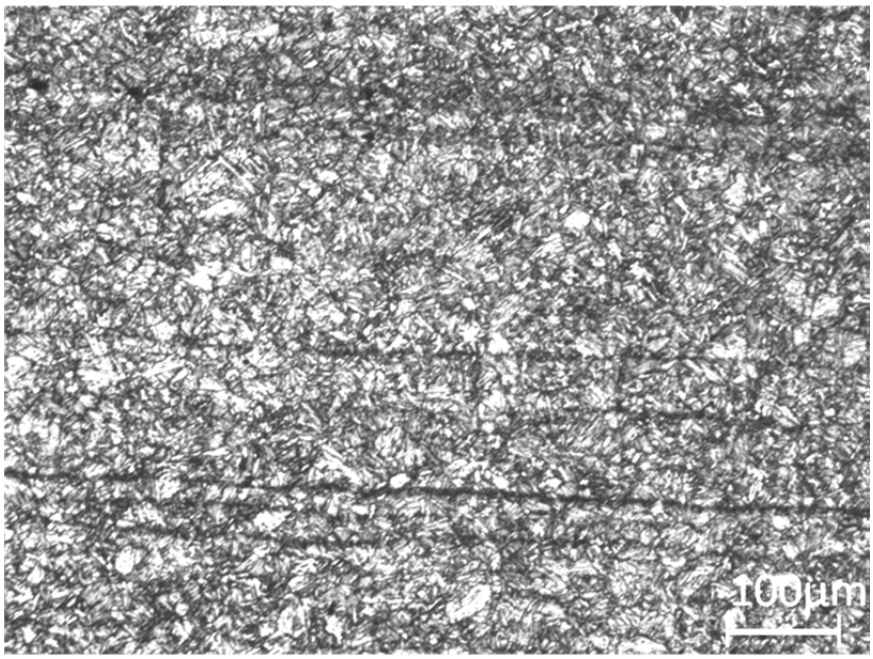

Figure 23. Optical micrograph from base material exhibiting tempered martensitic structure. The dark bands in the rolling direction are the inclusion stringers.

In the study of the base material, inclusion stringers were observed to be aligned along the rolling direction. The effect of these inclusion stringers on impact energy will be discussed later.

b. Dry Friction Stir Processing

(1) Transverse to FSW/P Direction. Shown in Figure 24 is a montage of the dry FSW/P stir zone starting with base material on the left, then moving across the TMAZ, then through the SZ, then through the right TMAZ, and finally into the other base material on the right. In this figure, the pin profile is overlaid and the flow pattern of material moving around the tool can be seen just outside the pin profile. The microstructure in the base metal is tempered martensite as shown in Figure 25. Prior austenite grains can be seen with plate-shaped martensite within them. Notice that the microstructure in this region is identical to that of the base material shown in Figure 23.

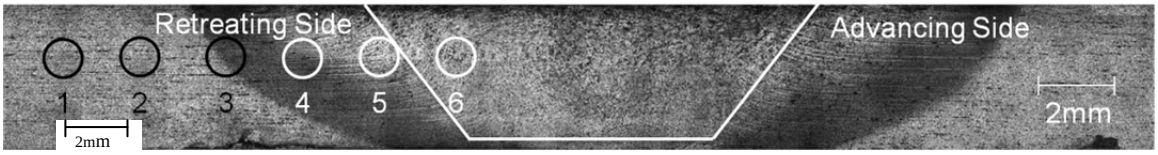

Figure 24. Montage of optical micrographs from etched dry FSW/P sample illustrating BM, TMAZ, and SZ. Higher magnification micrographs from areas within the circles 1 to 6 will be discussed in later figures.

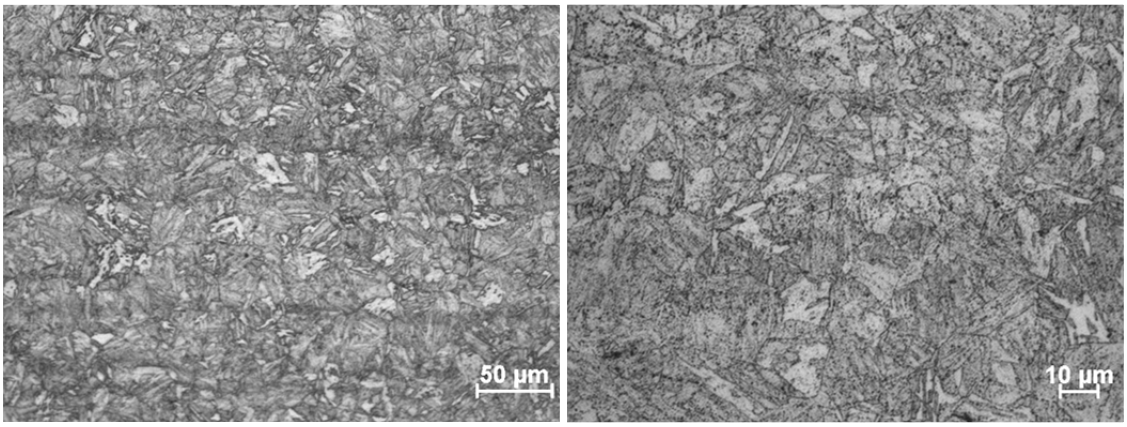

Figure 25. Optical micrograph of base material sample showing tempered martensitic microstructure at two magnifications from zone 1 of Figure 24.

The microstructure changes when approaching the TMAZ from a tempered martensitic microstructure in the base material to a refined, finer grained untempered martensitic microstructure, Figure 26. This occurs due to the local peak temperature produced by FSW/P and subsequent cooling rates. In addition to the heating

and cooling of the material to produce the aforementioned microstructure, it is hypothesized that the refined microstructure is the result of the severe plastic deformation of this process.

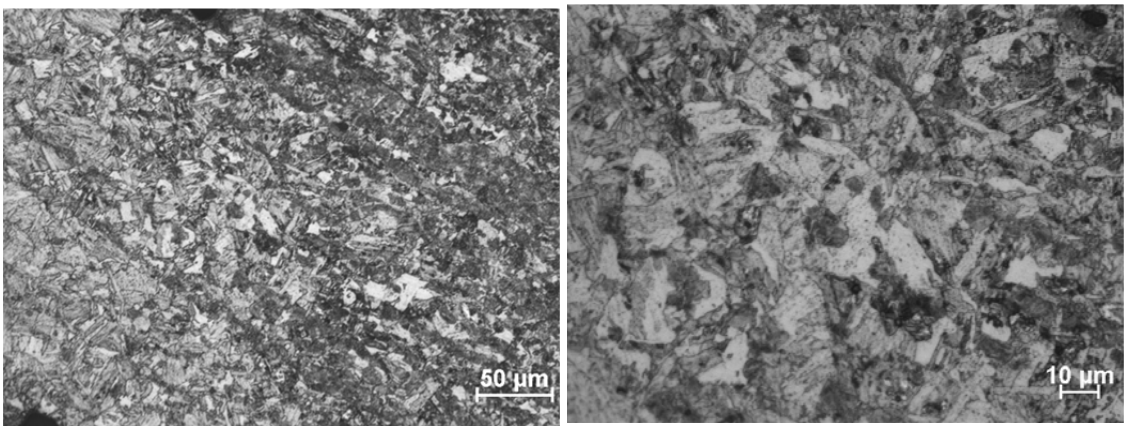

Figure 26. Optical microscopy from dry FSW/P TMAZ exhibiting refined martensitic microstructure from zone 3 in Figure 24.

The microstructure in Figure 27 shows coarse untempered martensitic structure in the stir zone. This is seen by the larger prior austenitic grains transforming into the plate-shaped untempered martensite. The larger grains are due to the slower cooling rate in the stir zone.

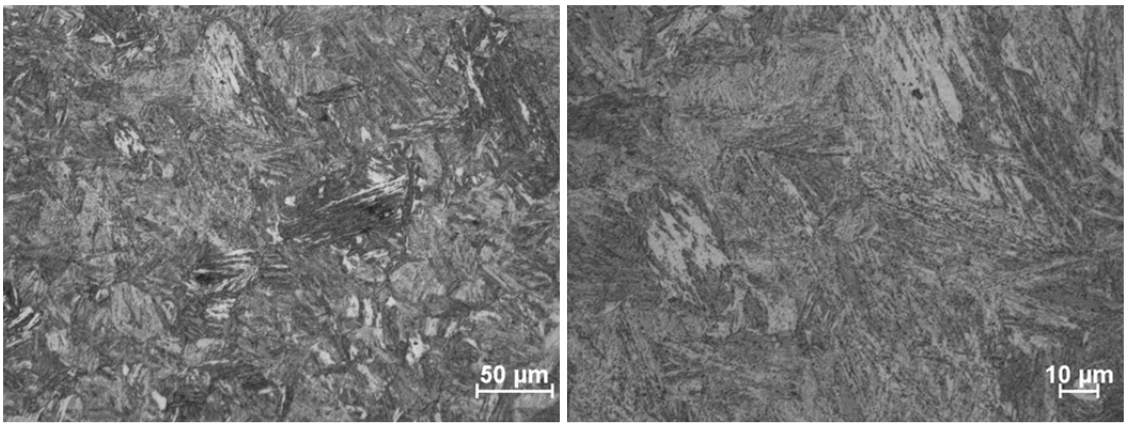

Figure 27. Optical microscopy from dry FSW/P stir zone showing coarse martensitic microstructure from zone 6 from Figure 24.

c. Underwater Friction Stir Processing

(1) Transverse to FSW/P Direction. The underwater FSW/P microstructure is similar to that seen in dry FSW/P. Shown in Figure 28 is a montage of the underwater FSW/P stir zone starting with base material on the left, then moving across the TMAZ, then through the stir zone, the through the right TMAZ, and finally into the base material on the right. Similar to the optical dry FSW/P montage, the pin profile overlaid on the montage shows the flow pattern of the material moving around the tool. The microstructure in this zone is that of tempered martensite as shown in Figure 29 and is identical to that of Figure 23. Prior austenite grains can be clearly seen with plate-shaped martensite grains (Figure 29 right) and dark bands due to the elongated inclusion stringers in the rolling direction (Figure 29 left).

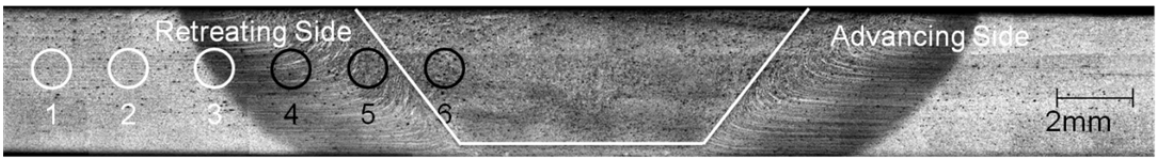

Figure 28. Optical micrograph from etched underwater FSW/P montage showing BM, TMAZ, and SZ. Higher magnification micrographs from areas within the circles 1 to 6 will be discussed in later figures.

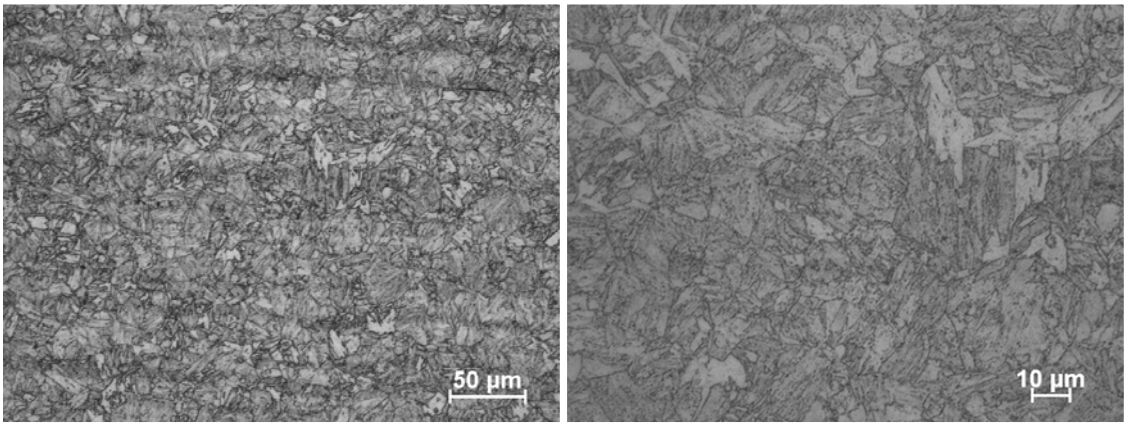

Figure 29. Optical micrograph from underwater base material exhibiting tempered martensitic microstructure and dark elongated bands due to inclusion stringers from zone 1 in Figure 28.

Similar to the dry FSW/P, the microstructure changes when approaching the TMAZ from tempered martensitic microstructure in the base material to refined smaller grained untempered martensitic microstructure, Figure 30. This occurs due to the local peak temperature produced by FSW/P and subsequent cooling rates. Again, the refined microstructure reflects the combination of local temperature and severe deformation of the FSW/P thermomechanical cycle. The differences between dry and underwater FSW/P microstructures are there is a more distinct boundary between the base material and the TMAZ. This is due to the higher cooling rates of the underwater FSW/P.

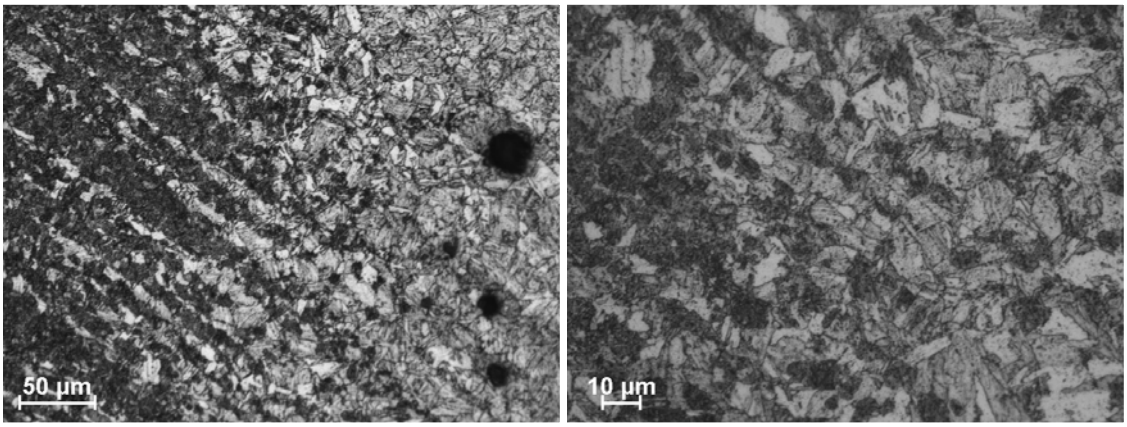

Figure 30. Optical microscopy from underwater FSW/P sample. TMAZ showing refined martensitic microstructure from zone 3 in Figure 28.

The microstructure in the stir zone is similar to that seen in the dry FSW/P stir zone. The microstructure seen in Figure 31 shows a coarse, untempered martensitic structure. This is seen by the larger prior austenitic grains transforming into the plate-shaped untempered martensite. The larger grains are due to the slower cooling rate in the stir zone. When compared to the dry FSW/P, the grain size of the untempered martensite is smaller. This occurs due to the quicker cooling rates associated with underwater FSW/P. The stir zone is quenched faster due to contact with the water.

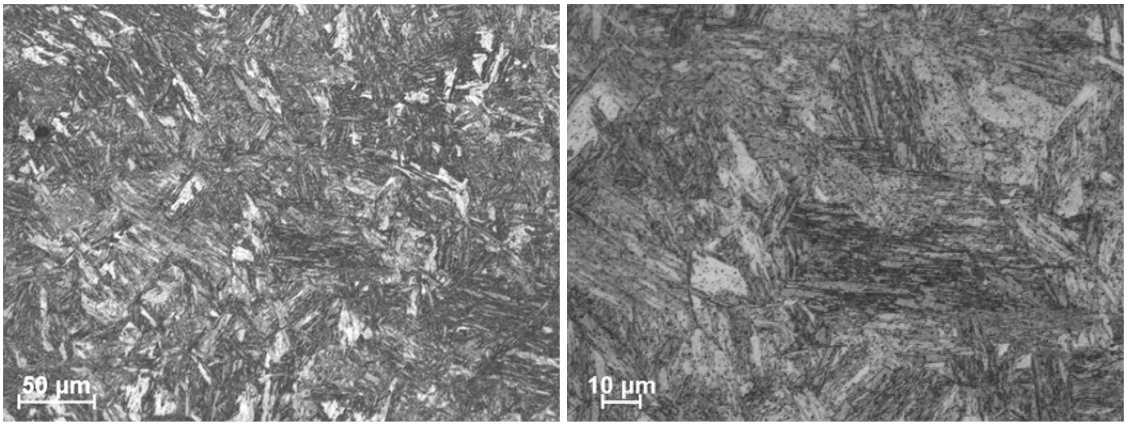

Figure 31. Optical micrograph from underwater FSW/P sample stir zone exhibiting coarse martensitic microstructure from zone 6 in Figure 28.

An important observation was the difference in the size of the stir nugget between the dry and underwater FSW/P. As shown in Figure 32, there is approximately a 2 mm difference in the extent of the SZ/TMAZ. It is also observed that the flow around the tool exhibits more distinct gradients in the underwater FSW/P than in the dry FSW/P. This can be attributed to the faster cooling rates associated with underwater FSW/P.

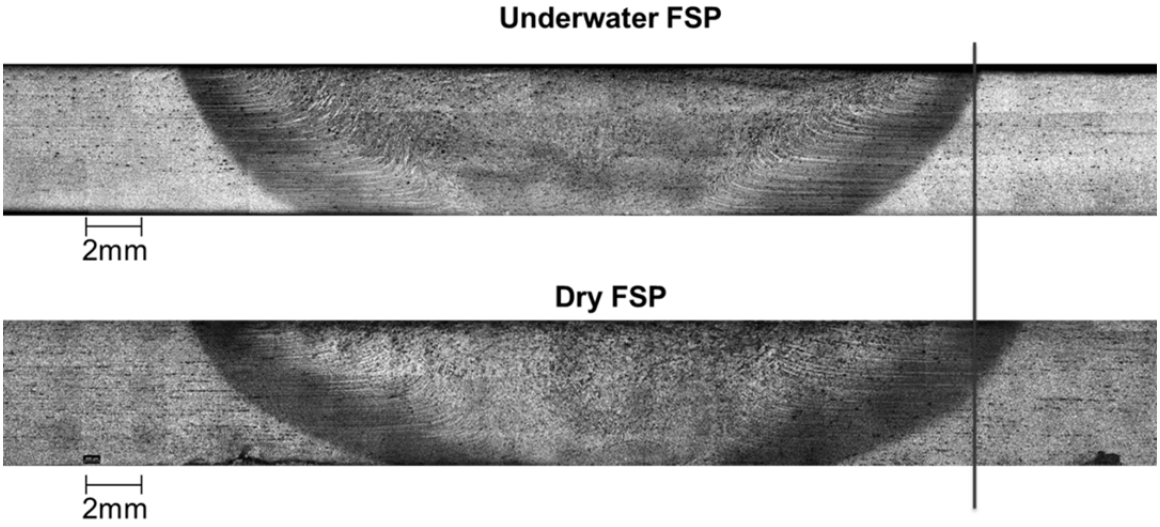

Figure 32. Optical micrograph montages for comparison of dry FSW/P vs. underwater FSW/P.

d. Pin Extraction Zones

A plan view montage of the pin extraction site for the dry FSW/P can be seen in Figure 33. Higher magnification micrographs were taken from the stir zone (zone 1), through the TMAZ (zone 4) and into the base material (zone 5 and 6). The flow pattern of the material moving around the tool can be seen in the plan view but not to the extent of that in the transverse view. Future studies require examining the microstructure of the plan view for mechanical deformation with respect to depth.

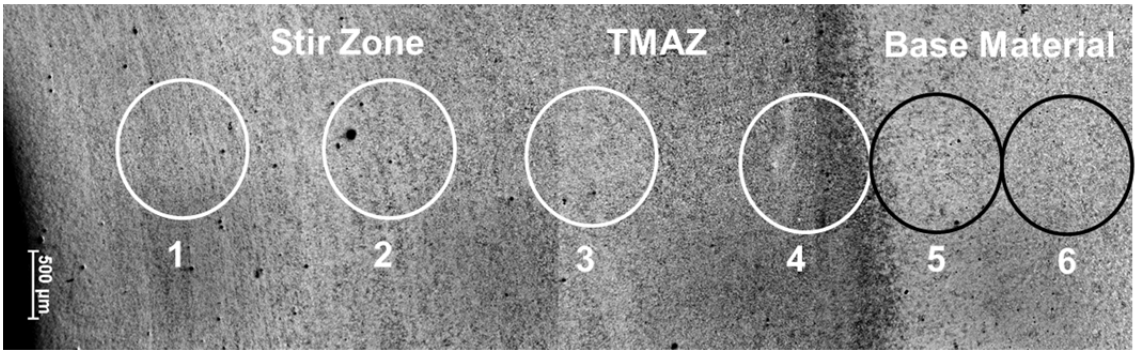

Figure 33. Montage of optical micrographs from the tool extraction site showing the microstructure ahead of the tool traverse direction from dry FSW/P sample. The tool extraction site can be seen at the far left end and higher magnification micrographs from areas within the circles 1 to 6 will be discussed in later figures.

The microstructure seen in Figure 34 shows a coarse untempered martensitic structure in the stir zone. This is seen by the large prior austenitic grains that have transformed into the plate-shaped untempered martensite. The larger grains are due to the slower cooling rate in the stir zone.

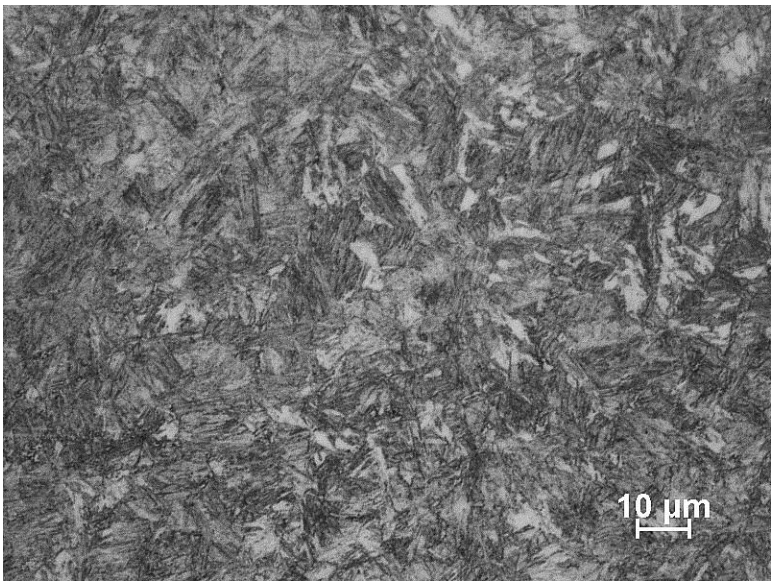

Figure 34. Optical micrograph from plan view of SZ for dry FSW/P, zone 1 in Figure 33.

In the plan view, the microstructure undergoes a change when approaching the TMAZ. The microstructure changes from a tempered martensitic structure to a refined smaller grained untempered martensitic structure, Figure 35. This transformation occurs due to the change in temperature produced by FSW/P and cooling rates.

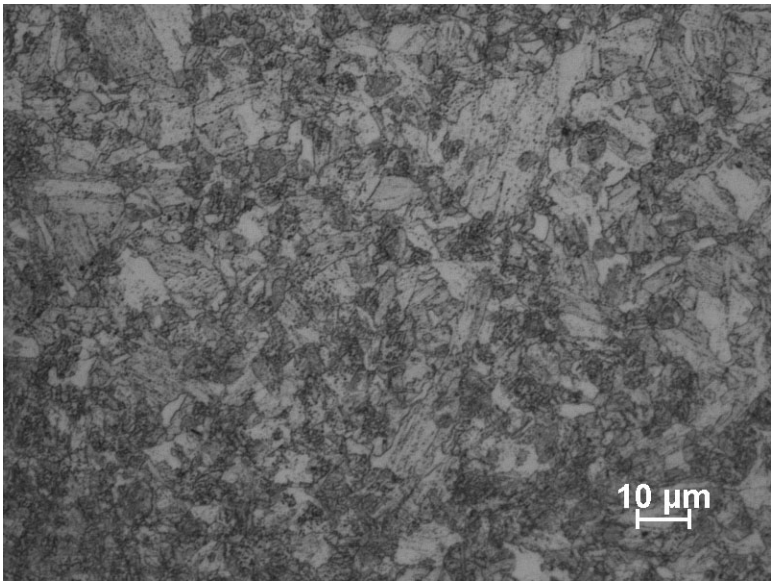

Figure 35. Optical micrograph from plan view of the TMAZ for dry FSW/P, zone 4 in Figure 33.

The base material shown in the plan view depicts prior austenitic grains transformed into tempered martensite, Figure 36. This is similar to the base material micrographs in the transverse direction.

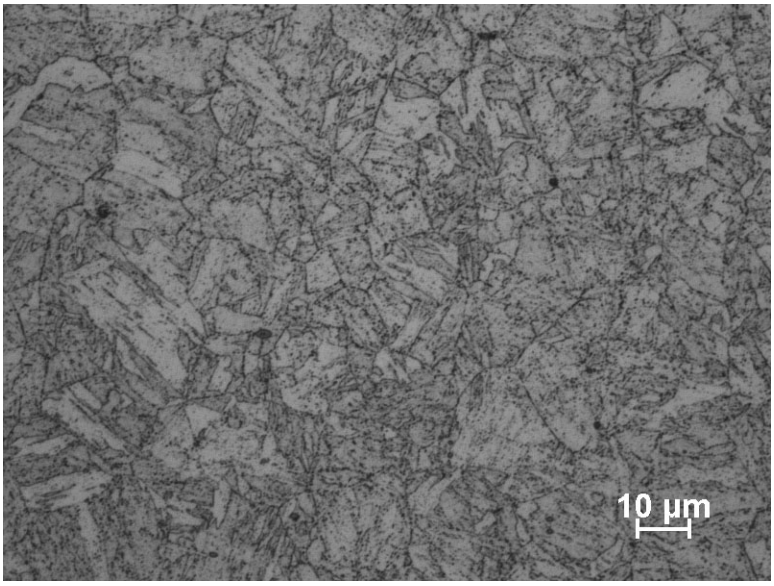

Figure 36. Optical micrograph from Plan view of base material for dry FSW/P, zone 6 in Figure 33.

A plan view montage of the pin extraction zone for the underwater FSW/P can be seen in Figure 37. Higher magnification micrographs were taken from the stir zone (zone 1), through the TMAZ (zone 3) and into the base material (zone 5 and 6). The flow pattern of the material moving around the tool can be seen in the plan view but not to the extent of that in the transverse view. Future studies require examining the microstructure of the plan view for mechanical deformation with respect to depth.

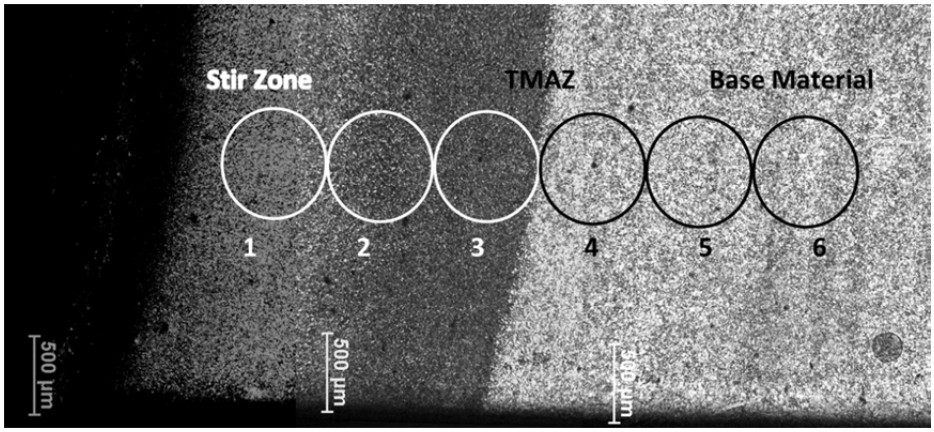

Figure 37. Montage of optical micrographs from the tool extraction site showing the microstructure ahead of the tool traverse direction from underwater FSW/P sample. The tool extraction site can be seen at the far left end and higher magnification micrographs from areas within the circles 1 to 6 will be discussed in later figures.

The stir zone observed in the plan view shows the coarse martensitic structure in the untempered condition, Figure 38. Large prior austenitic grains are transformed into the plate shaped untempered martensite. The large grains are due to the slower cooling rate in the stir zone. When compared to the dry FSW/P, the grain size of the untempered martensite is smaller. This is due to the quicker cooling rates associated with underwater FSW/P. The stir zone is quenched faster due to contact with the water.

Figure 38. Optical micrograph from Plan view of SZ for underwater FSW/P, zone 1 in Figure 37.

In the plan view, the microstructure clearly indicates that a phase change occurs at the edge of the TMAZ. The microstructure changes from a tempered martensitic structure in the base material into a refined, finer grained and untempered martensitic structure in the TMAZ, Figure 39. This is attributed to the change in temperature produced by FSW/P and cooling rates.

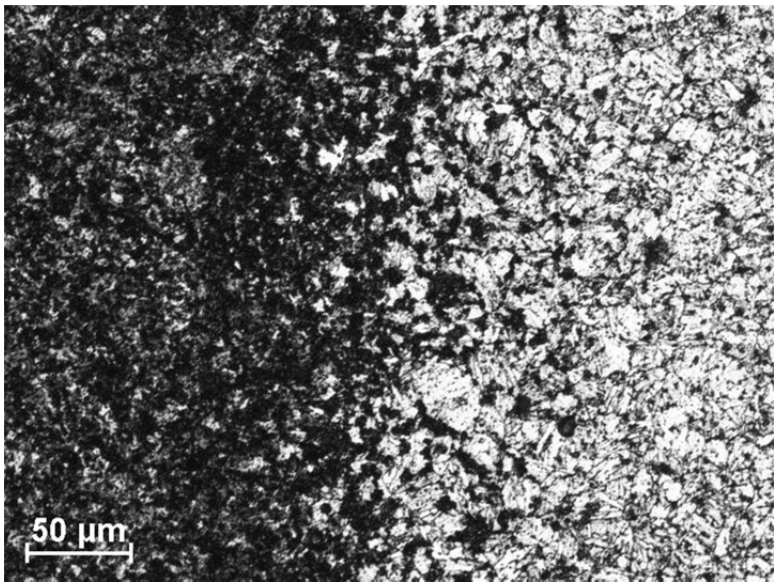

Figure 39. Optical micrograph from plan view of TMAZ for underwater FSW/P, zone 3 in Figure 37.

The plan view of the base material microstructure of underwater FSW/P is similar to that seen in dry FSW/P. The microstructure in this zone is that of tempered martensite as shown in Figure 40. Former austenite grains can be seen with plate-shaped martensite grains inside them.

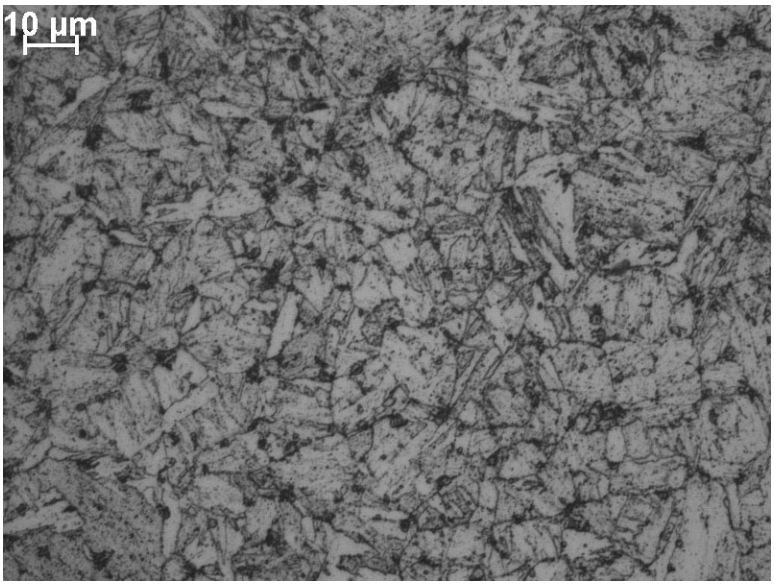

Figure 40. Optical micrograph from plan view of base material for underwater FSW/P, zone 6 in Figure 37.

One of the key observations made in this work was that there was no change in the shape of the grains near the TMAZ/SZ boundary unlike that reported in aluminum or bronze. The grains remain equi-axed and not elongated due to deformation.

2. Scanning Electron Microscopy

a. Base Material

Using the SEM, the base material was analyzed at higher magnifications. The tempered martensitic structure and carbides are clearly shown in Figure 41. The base material had inclusion stringers elongated in the rolling direction as shown in Figure 42. Inclusions, such as MnS that are presumably very plastic at the hot rolling temperature, become elongated in the rolling direction. The morphology of these inclusions has an effect on the mechanical properties of HY-80 similar to a fiber in a composite material.

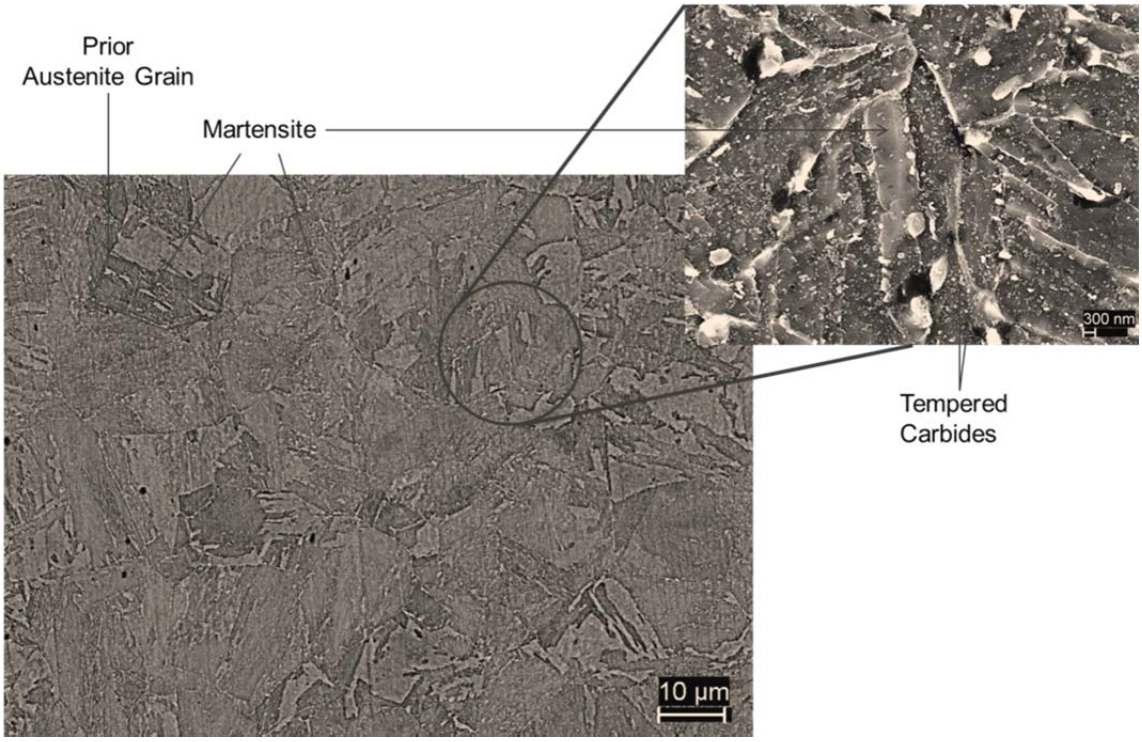

Figure 41. Secondary electron image from the base material showing the appearance of martensitic phase with tempered carbides. Higher magnification micrograph from encircled area clearly shows the distribution of tempered carbides.

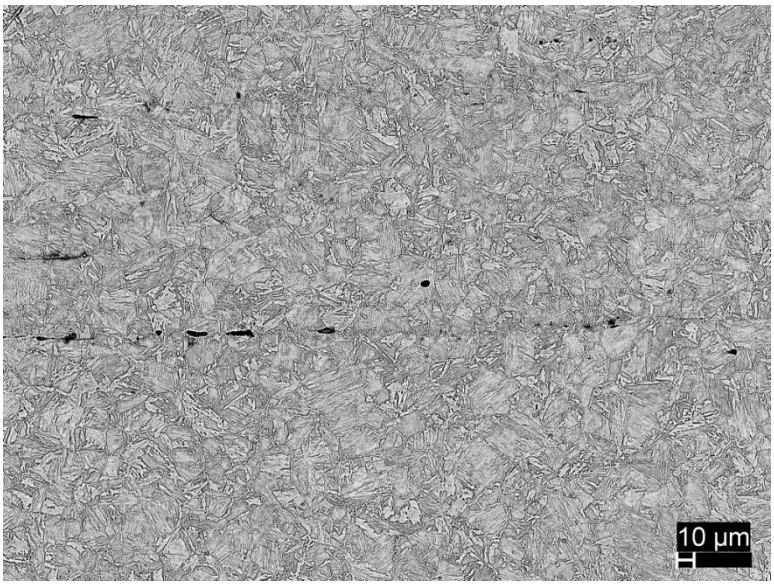

Figure 42. Back scattered electron image of base material showing the appearance of elongated inclusions in rolling direction.

At higher magnification, the inclusion stringers are observed to be elongated in the rolling direction, Figure 43, and have a ribbon-like shape when looked at from the transverse direction, Figure 44. Using energy dispersion spectroscopy (EDS), the inclusion stringers were analyzed to be MnS. Figure 45 shows secondary electron images from the rolling and transverse directions of an inclusion stringer and typical X-ray spectra from inclusions demonstrate that they are predominantly MnS, though small amounts of oxide/silicates also appear to be present. Elemental mapping (shown on the right side of Figure 45) revealed that inclusions are comprised of MnS.

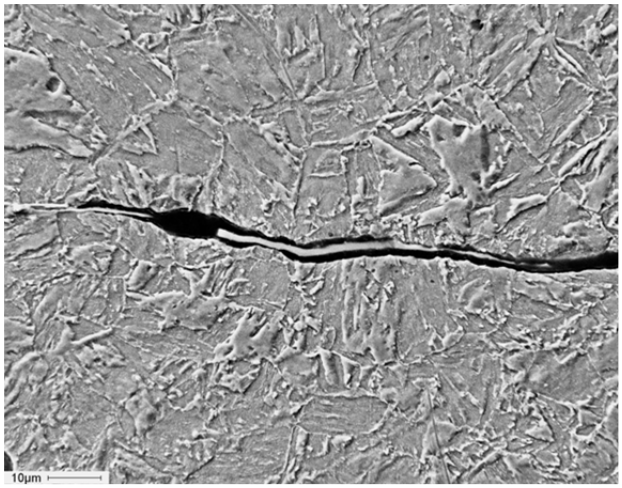

Figure 43. Secondary electron image of inclusion stringer in BM as observed in the rolling direction.

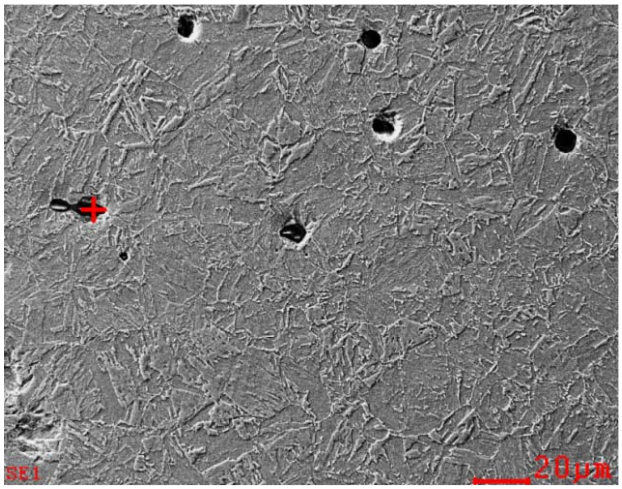

Figure 44. Secondary electron image of inclusions observed from the transverse direction showing a ribbon like morphology.

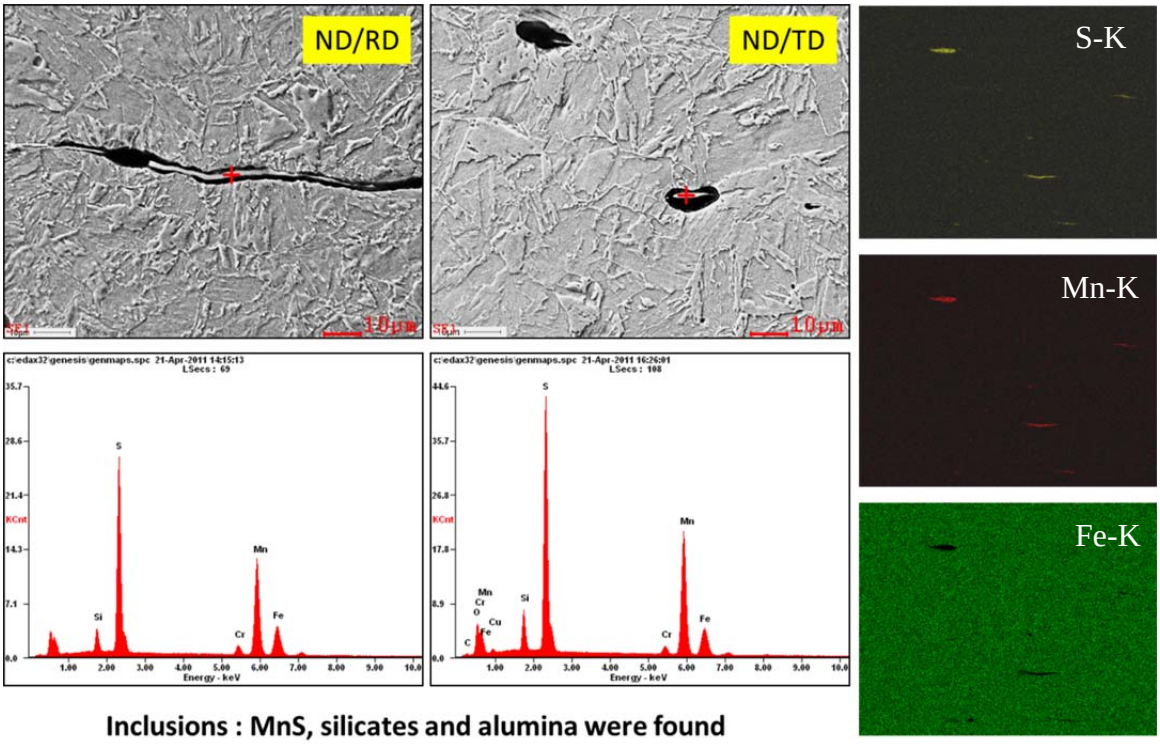

Figure 45. Secondary electron images from the rolling and transverse directions of an inclusion stringer and typical X-ray spectra from inclusions demonstrate that they are predominantly MnS, though small amounts of oxide/silicates also appear to be present. ND/RD refers to the normal direction, RD rolling direction, TD. Transverse direction. Right side shows X-ray elemental mapping of the distribution of the indicated elements.

b. Dry Friction Stir Processing

(1) Transverse to FSW/P Direction. When approaching the TMAZ, the microstructural changes from tempered martensitic in the base material to the fine grained untempered martensitic microstructure in the TMAZ is clearly seen in the SEM micrograph shown in Figure 46. This observation is consistent with the optical microscopy results.

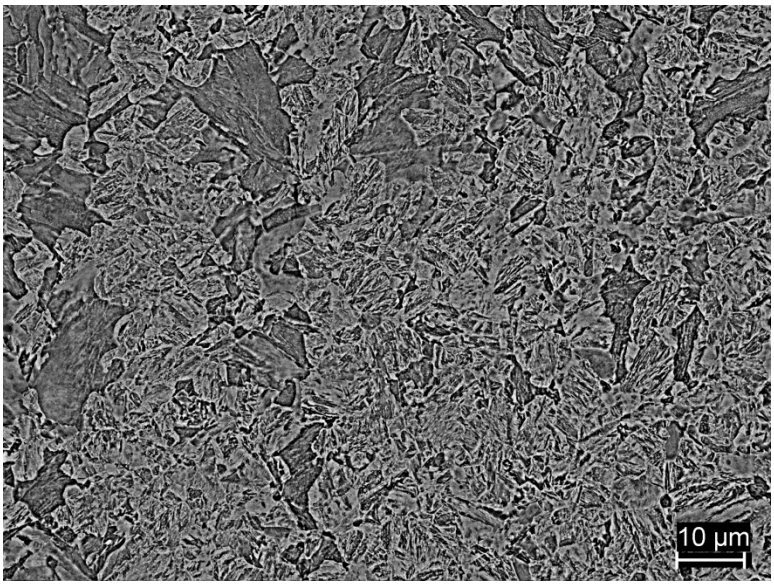

Figure 46. Back scattered electron image of TMAZ of dry FSW/P displaying fine martensitic microstructure.

The microstructure seen in Figure 47 shows a coarse untempered martensitic structure present in the stir zone. This is seen by the plate-shaped untempered martensite. The larger grains are due to the slower cooling rate in the stir zone than in the TMAZ.

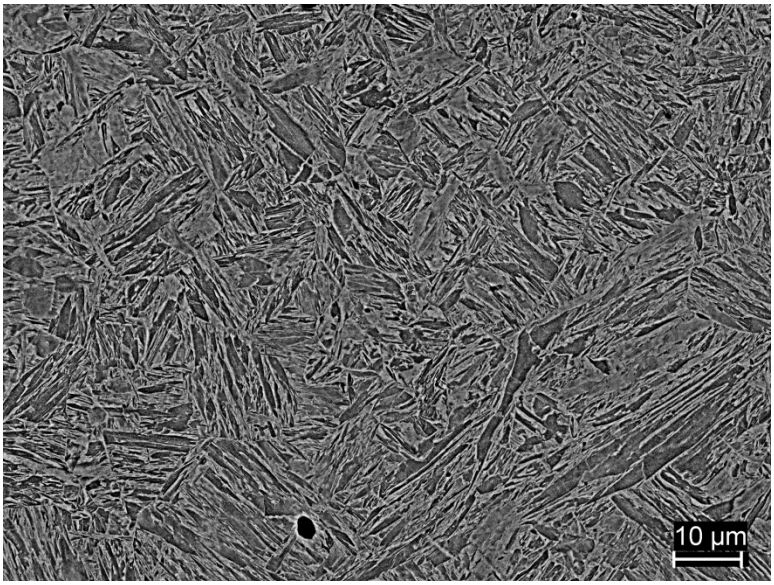

Figure 47. Back scattered electron image of the stir zone of dry FSW/P displaying coarse martensite.

c. Underwater Friction Stir Processing

(1) Transverse to FSW/P Direction. The variation of the microstructures from the base material to the TMAZ is very similar to that observed from the dry FSW/P. The microstructure in the TMAZ is a refined finer grained untempered martensitic microstructure, Figure 48. Again, this reflects the FSW/P thermomechanical cycle. This is due to the quicker cooling rates of the underwater FSW/P, where the TMAZ is quenched faster due to contact with the water.

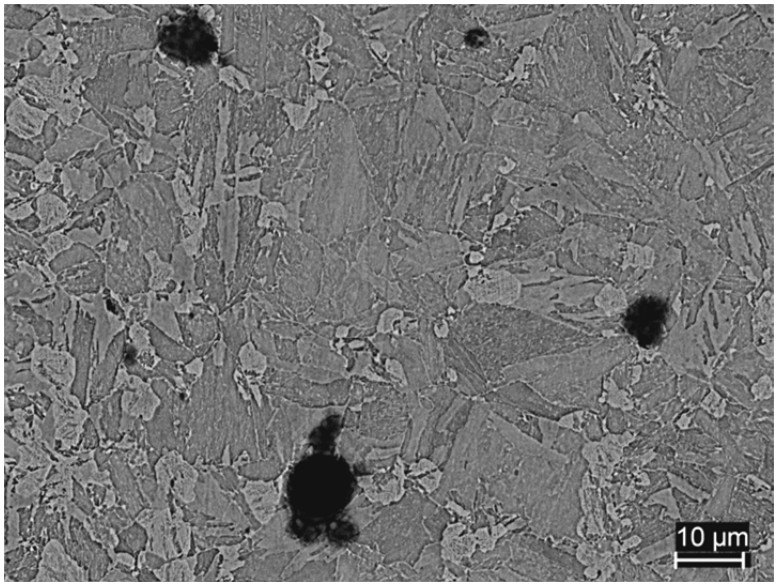

Figure 48. Back scattered electron image of the TMAZ of underwater FSW/P.

As mentioned before, the microstructure in the underwater FSW/P stir zone is similar to the dry FSW/P stir zone. Figure 49 exhibits a coarse untempered martensitic microstructure. This is indicated by the large prior austenitic grains transforming into the plate-shaped untempered martensite. When compared to the dry FSW/P, the grain size of the untempered martensite is smaller. This occurs due to the quicker cooling rates associated with underwater FSW/P, where the stir zone is quenched faster due to contact with water.

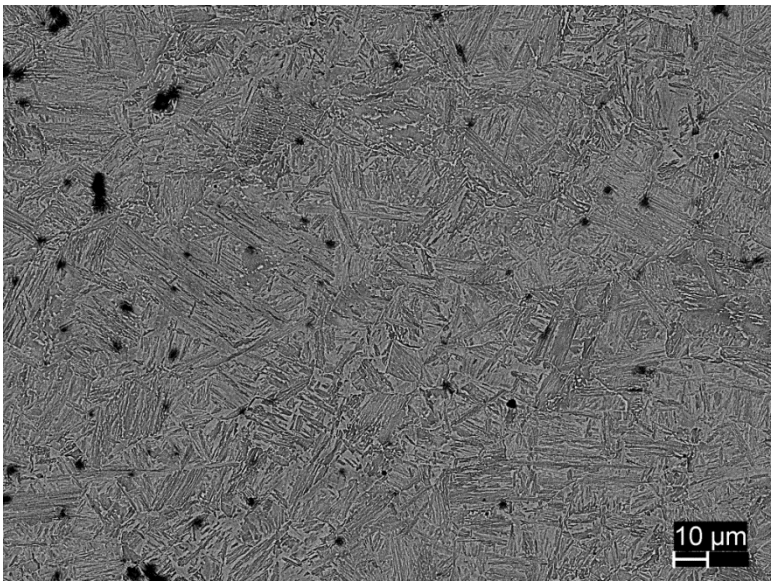

Figure 49. Back scattered electron image of the stir zone of underwater FSW/P.

It is noteworthy to mention that there were no signs of elongated inclusion stringers in both the dry and underwater FSW/P samples. This observation suggests that the long inclusion stringers were redistributed as very fine particles. Further high resolution microscopy is required to examine the nature of these inclusions.

d. Fractography

The fracture surface of the Charpy sample tested at -80°C, is shown in Figure 50. The dimple morphology observed in this fractograph indicated that ductile failure of the material occurred by micro void coalescence, or the “tearing” of the material.

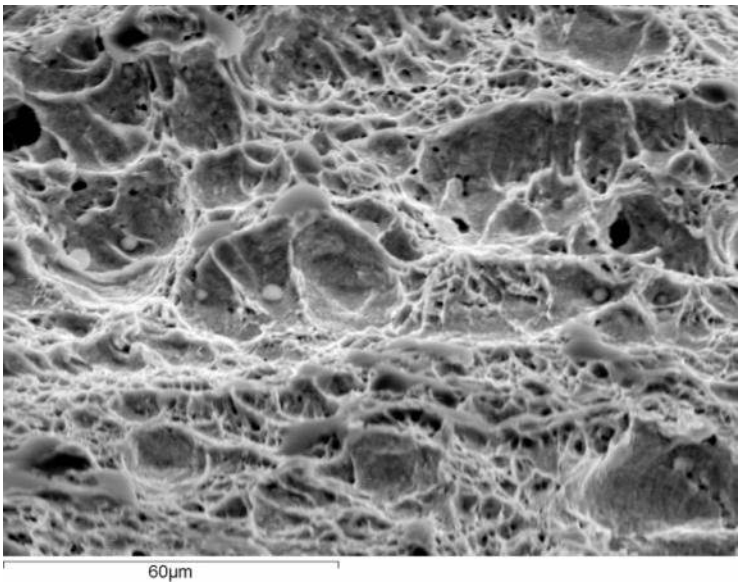

Figure 50. Fractograph secondary electron image of base material showing micro void coalescence.

The fracture surface morphology of the dry FSW/P sample demonstrates that the material failed in a predominantly ductile mode, Figure 51. The Charpy sample was tested at -80°C. Dimples can be seen suggesting fracture by micro void coalescence, but with some cleavage cracking, especially at the center-right in this image. The cleavage cracking is a sign of brittle failure.

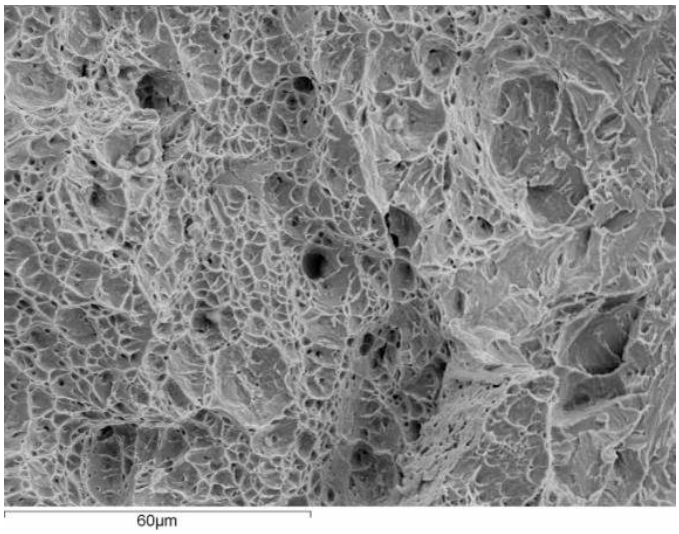

Figure 51. Secondary electron image showing fractograph of dry FSW/P with micro void coalescence and cleavage cracking.

Finally, underwater FSW/P sample fractography demonstrates that the material is failing in a more nearly brittle mode. A fractograph from this Charpy sample tested at -80°C, seen in Figure 52, shows that cleavage cracking is prevalent compared to base material and dry FSW/P material. Brittle failure would be unacceptable for submarine application and further research will have to be conducted to control microstructure through control of cooling rates and thereby increase ductility.

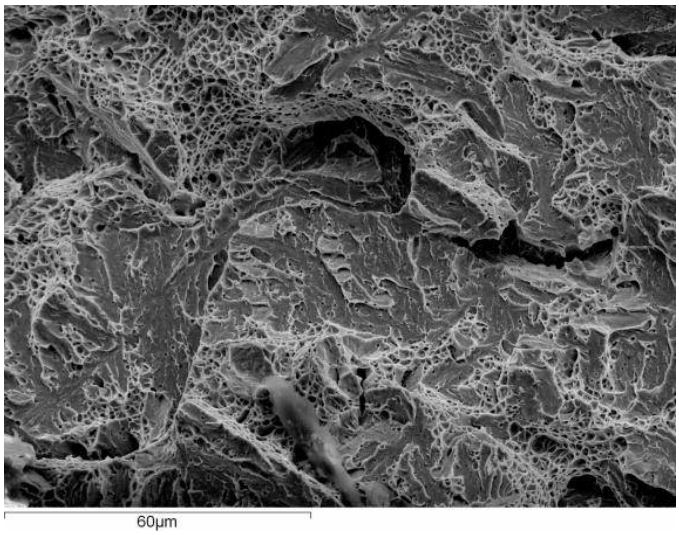

Figure 52. Secondary electron image showing fractograph of underwater FSW/P with cleavage cracking.

D. MECHANICAL PROPERTIES

1. Impact Energy

a. Base Material

Base material was subjected to Charpy V-Notch Impact testing to determine the Ductile to Brittle Transition Temperature (DBTT). This was to establish a baseline to compare the effects of FSW/P on the impact resistance of HY-80. As shown in Figure 53, the Charpy energy is higher in samples where the crack propagation is perpendicular to the rolling direction. It is believed that the crack crosses the inclusion stringers and therefor results in higher impact energy for transverse samples in such a crack-divider mode of propagation. The rolling direction samples, where the crack propagation runs parallel to the inclusion stringers, had lower impact energy. When the crack propagates parallel to the inclusion stringer, it follows a low-energy crack path and therefore exhibits a lower impact energy. It must be noted that when the data presented in this thesis is compared to that of the Navy Ship Systems Conference [20] there is discrepancy between the data, appendix F. Their data shows that samples where the crack propagates normal to the rolling direction produces lower impact energy than that of samples orientated in the rolling direction. Further study is needed to fully understand the reasons behind the inconsistencies.

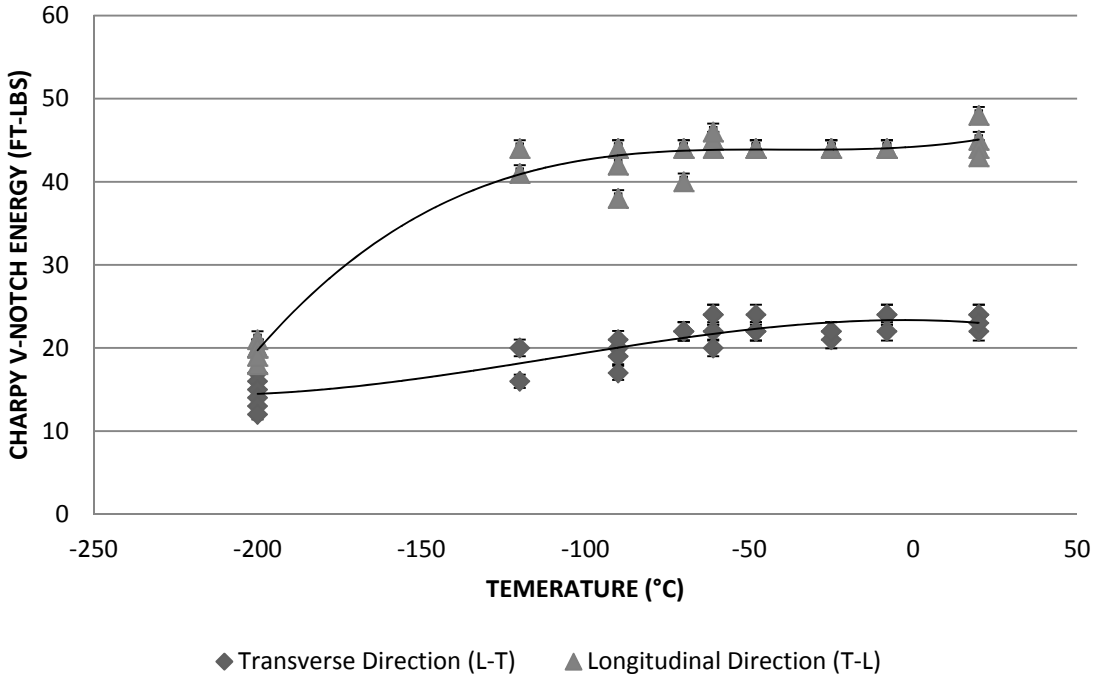

Figure 53. Comparative plot of impact energy for BM samples tested in the longitudinal and transverse directions to the rolling direction.

b. Dry and Underwater Friction Stir Processing

FSW/P Charpy Impact energy tests can be seen in Figure 54. From the data, the impact energy is higher in the friction stir welds done in ambient dry conditions than those done underwater. The lower impact energy in the underwater FSW/P can be due to the higher cooling rates and material being fully hardened by the untempered martensite in the stir zone.

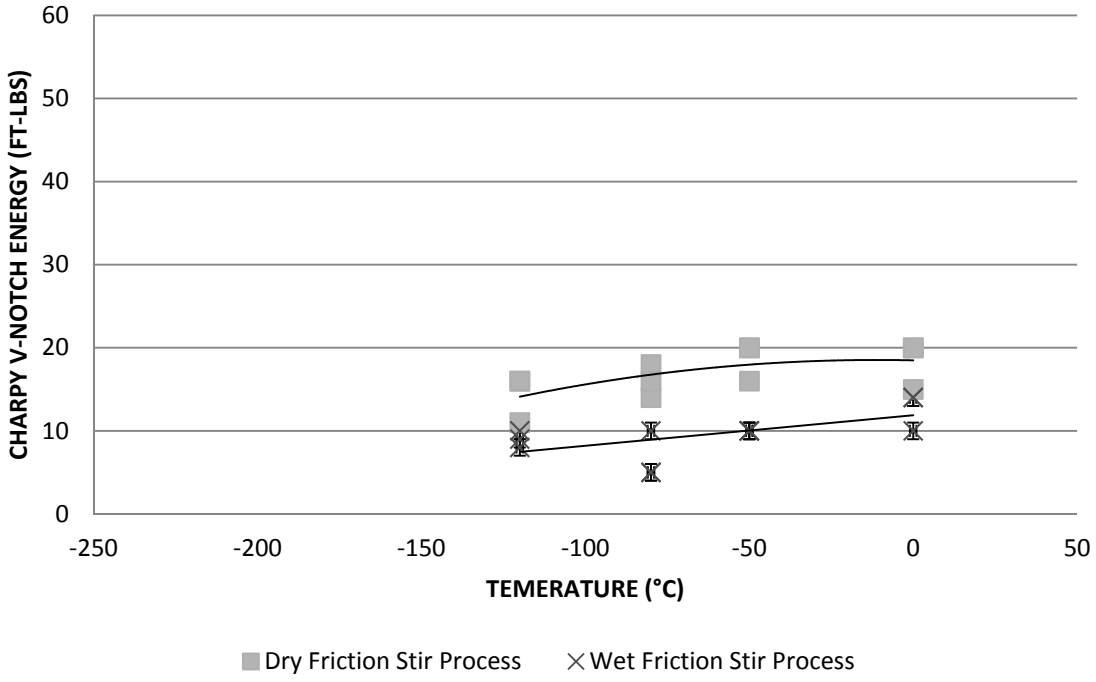

Figure 54. Comparative plot of Charpy impact energy for dry vs. underwater FSW/P.

Since the material is fully hardened due to the formation of untempered martensite, the Charpy Impact energy for FSW/P for both dry and wet FSW/P are less than that of the base material, Figure 55. However, the similarities between the two point to a ductile brittle transition temperature similar to the base material.

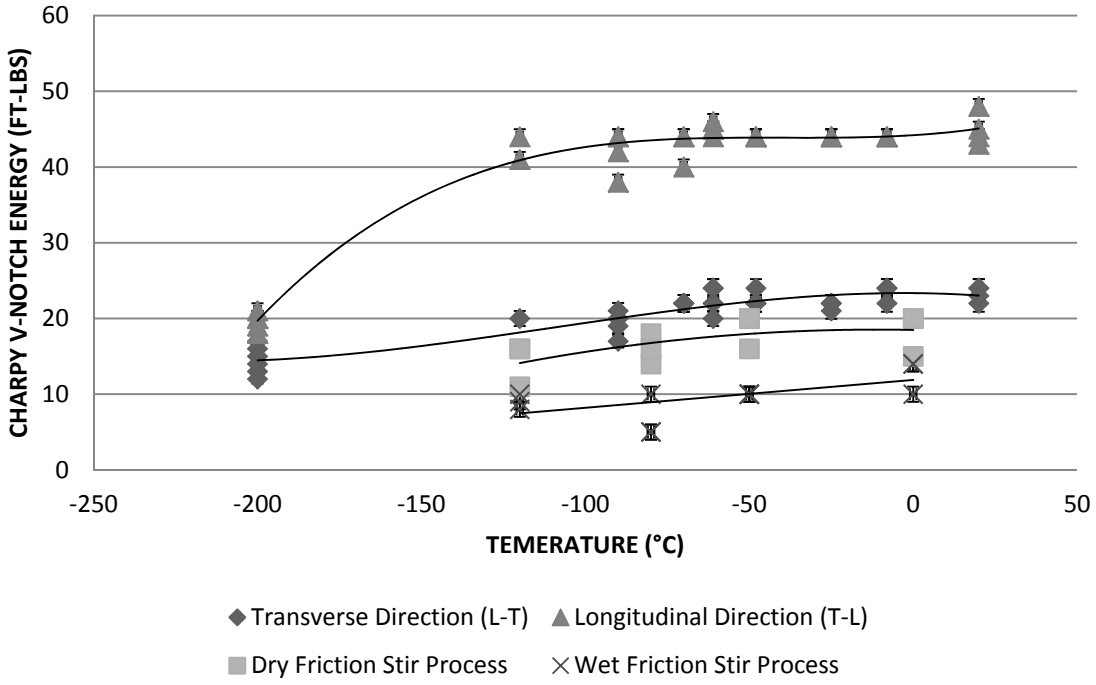

Figure 55. Comparative plot of Charpy impact energy for BM vs. dry and underwater FSW/P.

2. Tensile Strength

Tensile testing was conducted on base material in both the rolling direction and the transverse direction. No noticeable difference was determined between the two orientations. It was found that the base material had the yield strength around 750 MPa which is higher than the expected range of 550 MPa to 680 MPa of HY-80 steel. This value suggests that the material is HY-100. Further research is required to determine the cause of the abnormality. The tensile samples that had been FSW/P showed an increase in tensile strength, but a decrease in ductility, Figures 56 and 57. This was to be expected due to the transformation from tempered martensite to untempered martensite due to the heating of the material caused by FSW/P. In order to implement FSW/P, post heat treatment or tempering has to be done to reduce strength but obtain sufficient toughness similar to that of the base material.

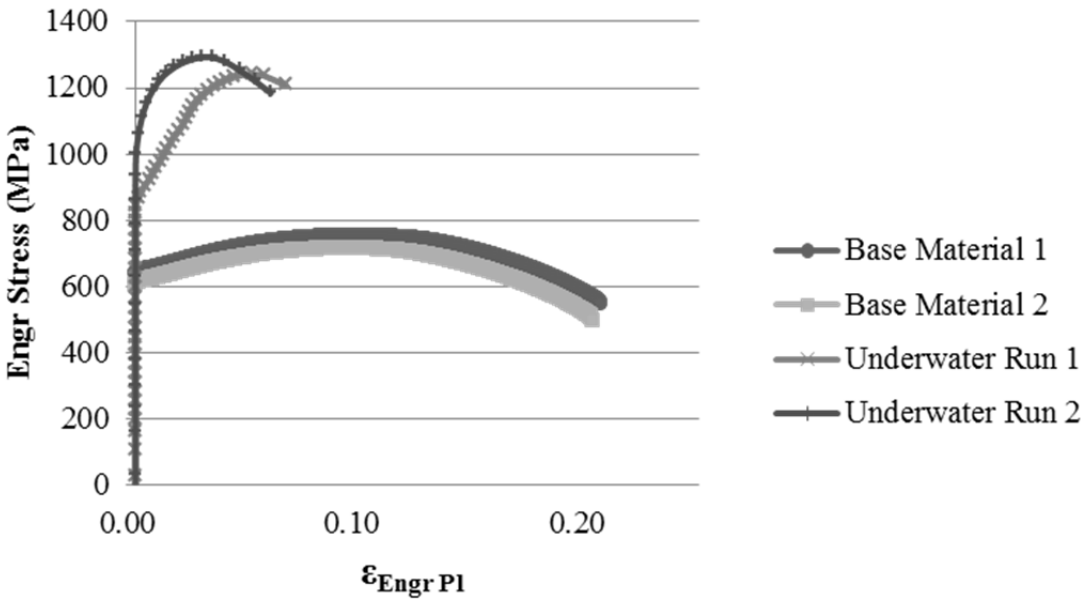

Figure 56. Comparison of underwater FSW/P to base material yield strength.

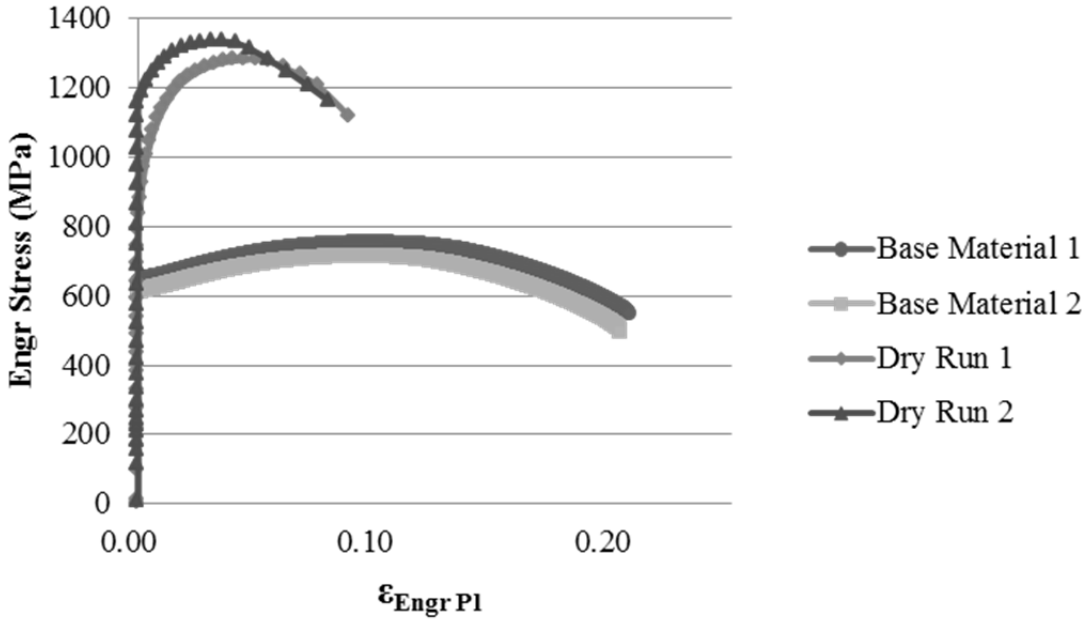

Figure 57. Comparison of dry FSW/P to base material yield strength.

3. Microhardness

Microhardness was used to summarize the findings of this thesis by showing the hardness changes associated with the martensitic microstructures produced by FSW/P. Base material values ranged from 200 to 250 on the diamond pyramid hardness scale (DPH). The variance is due to the non-homogenous nature of the material previously discussed (including porosity and inclusion stringers).

When approaching the TMAZ in the dry FSW/P microstructure, there is a gradual increase in hardness that peaks at around 380 to 400 DPH. The hardness reaches its maximum and stays constant across the stir nugget. Upon reaching the other TMAZ, the hardness gradually decreases until the microstructure becomes base material, Figure 58.

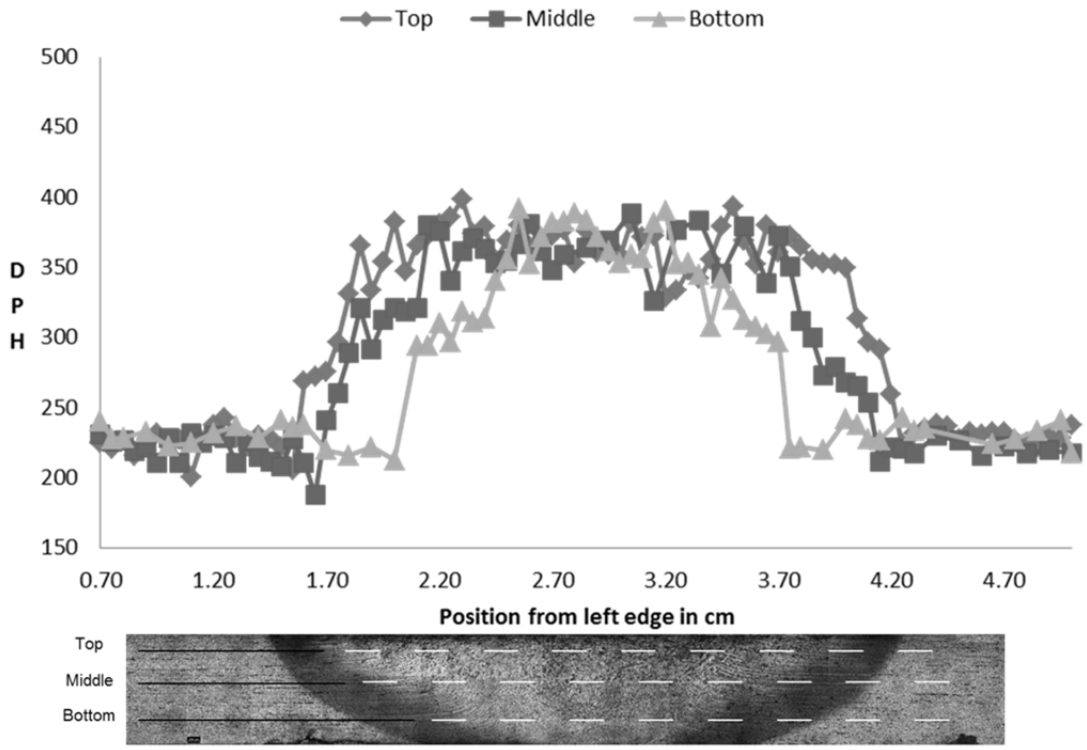

Figure 58. Dry FSW/P microhardness with respect to weld depth as indicated.

Examining the underwater FSW/P microhardness traverse, Figure 59, the differences are small when compared to that of the dry microhardness traverse. However, when approaching the TMAZ from the base material, the hardness increases at a steep slope. This represents the clear transition between tempered martensite and the

beginnings of the untempered martensite, which has been refined. Another difference from the dry FSW/P is the peak hardness across the stir nugget is 420 to 450 DPH. This signifies that the HY-80 is being fully austenitized and transforming to untempered martensite. These experimental results clearly indicate that in both the dry and underwater FSW/P complete austenitization occurs during processing and subsequently the austenite transforms to martensite upon rapid cooling. However, during the dry FSW/P, some tempering occurs due to the slower cooling rate compared to the quick quench of underwater FSW/P that retains the untempered martensite.

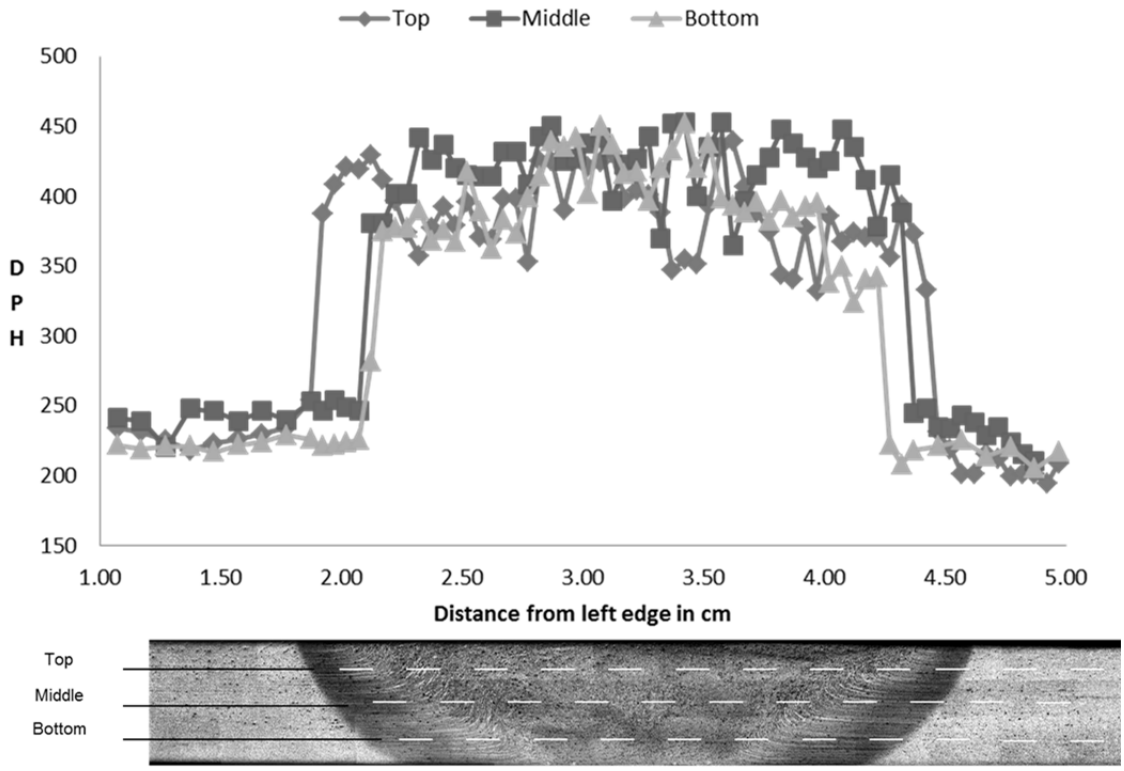

Figure 59. Underwater FSW/P microhardness with respect to weld depth as indicated.

This deduction is supported by hardness data of untempered martensite as reported by George Krauss [23]. Comparing the hardness measured from the underwater stir zones to the maximum hardness obtained from 0.18 wt% carbon, the conclusion can be made that the microstructure in the stir zone is untempered martensite, Figure 60. This

data are adapted from Krauss [23] and show the relationship between the maximum attainable hardness of martensite and carbon content of for Fe-C alloys.

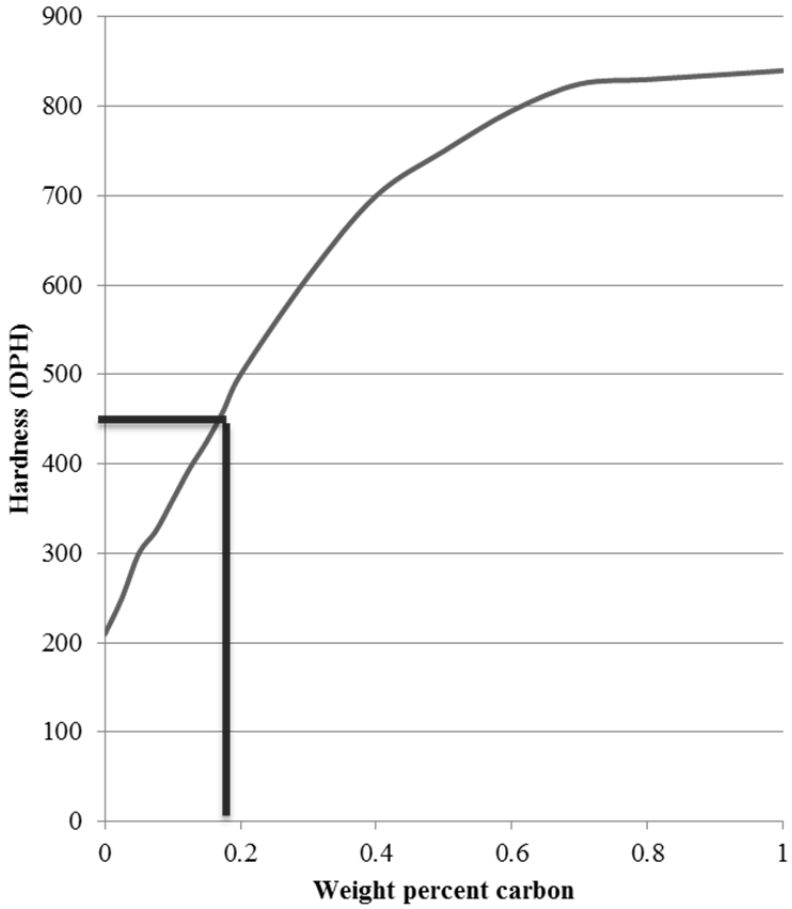

Figure 60. Re-plotted Maximum hardness of martensite as a function of carbon content in Fe-C alloys and steels.

V. CONCLUSIONS

A. SUMMARY OF THIS WORK

In this work, Friction stir processing was conducted on HY-80 underwater and dry. These welds were then sectioned, examined microscopically, and mechanically tested. These results were then compared to non FSW/P treated base metal to determine if FSW/P was feasible. The following conclusions were demonstrated:

- Friction Stir Processing/welding of HY-80 grade steels in both dry and underwater conditions is feasible while maintaining the hydrogen content within allowable levels
- The MnS inclusions appearing as elongated stringers in the hot rolled HY-80 plate are presumably broken up and distributed due to the thermomechanical processing of FSW/P
- Material is fully austenitized during FSW/P and transforms to martensite with the cooling rates established during both dry and underwater FSW/P.
- Deformation during FSW/P of HY-80 did not result in the elongation of the grains in the TMAZ region unlike that reported in aluminum alloys and Nickel Aluminum Bronze
- The martensite undergoes partial tempering in the dry FSW/P resulting in a lower hardness than that of underwater FSW/P in which the microstructure is untempered martensite and hence harder
- These microstructural features and the observation of some cleavage steps in FSW/P samples indicate that post-FSW/P tempering must be conducted to enhance the properties
- Charpy impact resistance, tensile testing, and microhardness data is in conformity with the microstructural observations mentioned above

B. FUTURE RESEARCH

Addition research is needed in an attempt to control cooling to control microstructure by tempering dry and underwater FSW/P runs. The experiment would require both the dry and underwater FSW/P welds to be heated to 1200°F and then quenching in either water or oil to bring the temperature rapidly down to retain the microstructure in a tempered martensitic state. These samples would then be subjected to Charpy V-Notch impact energy tests and compared to the results of the non-tempered dry

and underwater FSW/P welds. The goal would be to produce FSW/P welds with mechanical properties similar to base material.

The redistribution of inclusions in the stir zone and its effects on the microstructure and mechanical properties must be carefully studied.

APPENDIX A – LUVAK INC. REPORT

Luvak Inc.
722 Main Street
P.O. Box 597
Boylston, MA 01505
Phone 508-869-6401
www.luvak.com

Analytical report no.
0-61258
Page 1 of 1

Requested by:
Naval Postgraduate School
1 University Circle
Monterey, CA 93943

Attention:
Will Young
Jennifer Lee
jllee@nps.edu

Invoice number: 67563
Customer Purchase Order no.: Credit Card

Date received: 05/19/11
Report date: 05/27/11
Invoice date: pending

Description: Three Steel samples were analyzed as listed below.

Results:

Sample Identification	Base	Wet	Dry
	ppm	ppm	ppm
Hydrogen	1.9	2.3	0.9
	%		
Carbon	.456	---	---
Sulfur	.028	---	---
Phosphorus	.009	---	---
Silicon	.25	---	---
Nickel	.072	---	---
Chromium	.83	---	---
Molybdenum	.17	---	---
Vanadium	.008	---	---
Magnesium	<.0005	---	---

Methods: Carbon & Sulfur - Combustion infrared detection - ASTM E 1019-08
Hydrogen - Vacuum hot extraction - ASTM E 146-83
All others - Direct current plasma emission spectroscopy - ASTM E 1097-07

Luvak Inc.
By
Derek Langlois
Quality Manger

THIS PAGE INTENTIONALLY LEFT BLANK

APPENDIX B – OPTICAL MICROGRAPHS OF DRY FSW/P

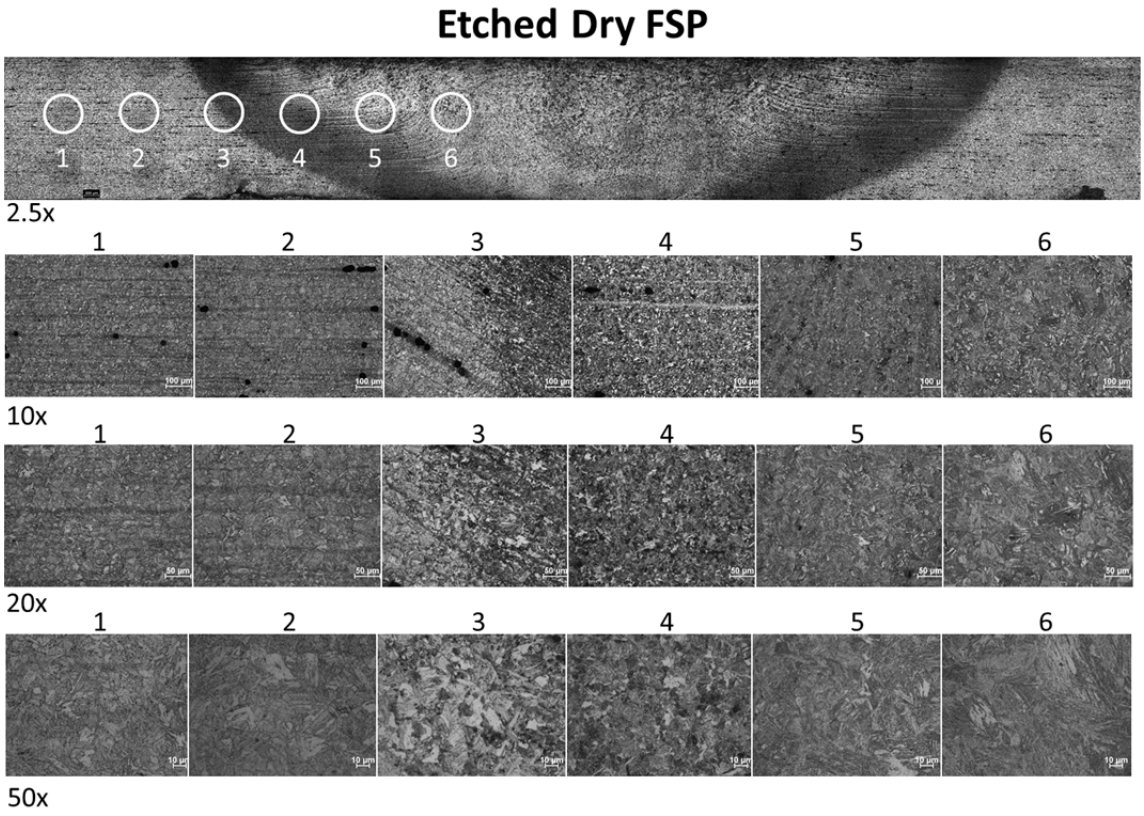

THIS PAGE INTENTIONALLY LEFT BLANK

APPENDIX C – OPTICAL MICROGRAPHS OF UNDERWATER FSW/P

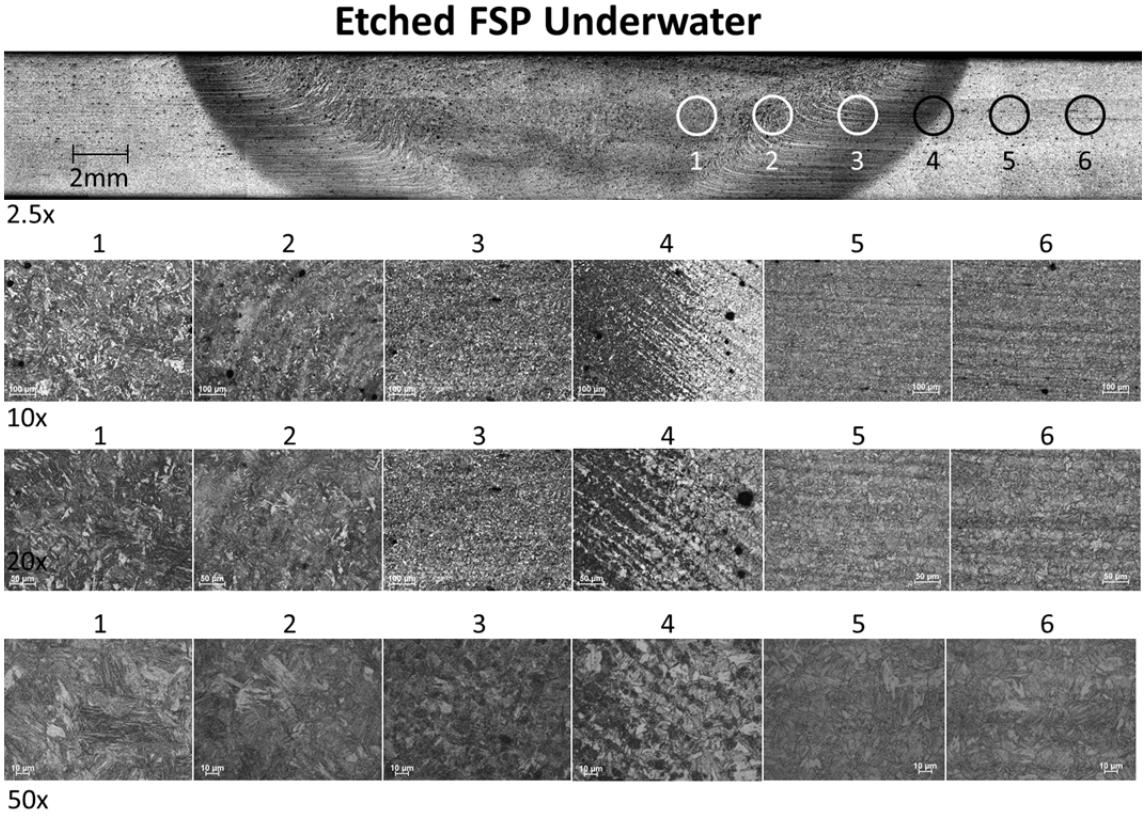

THIS PAGE INTENTIONALLY LEFT BLANK

APPENDIX D – INDIVIDUAL TENSILE TESTS

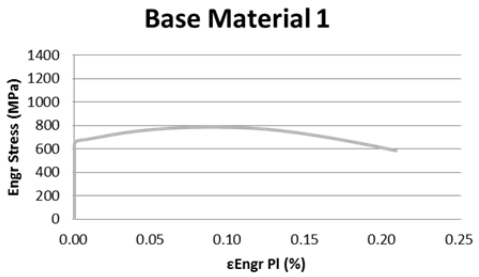

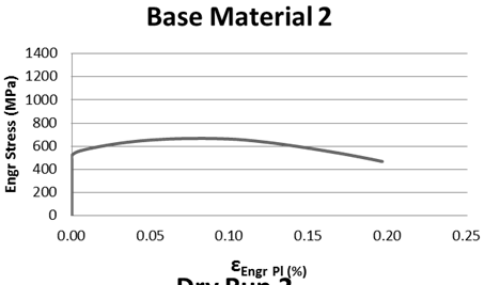

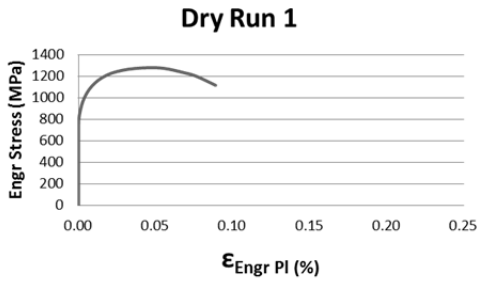

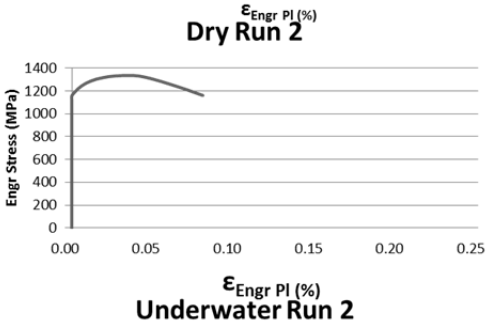

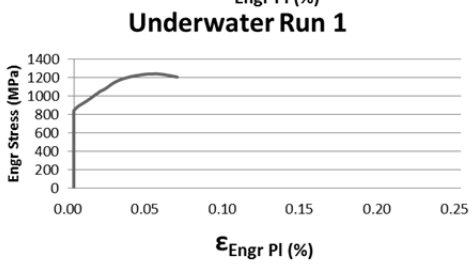

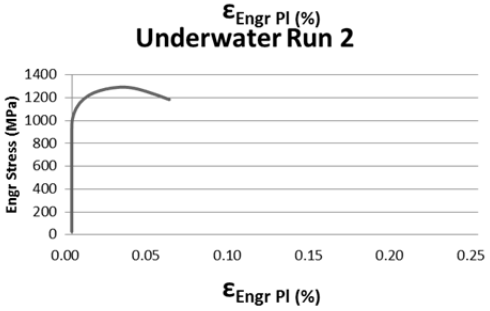

THIS PAGE INTENTIONALLY LEFT BLANK

APPENDIX E – TENSILE STRENGTH COMBINED

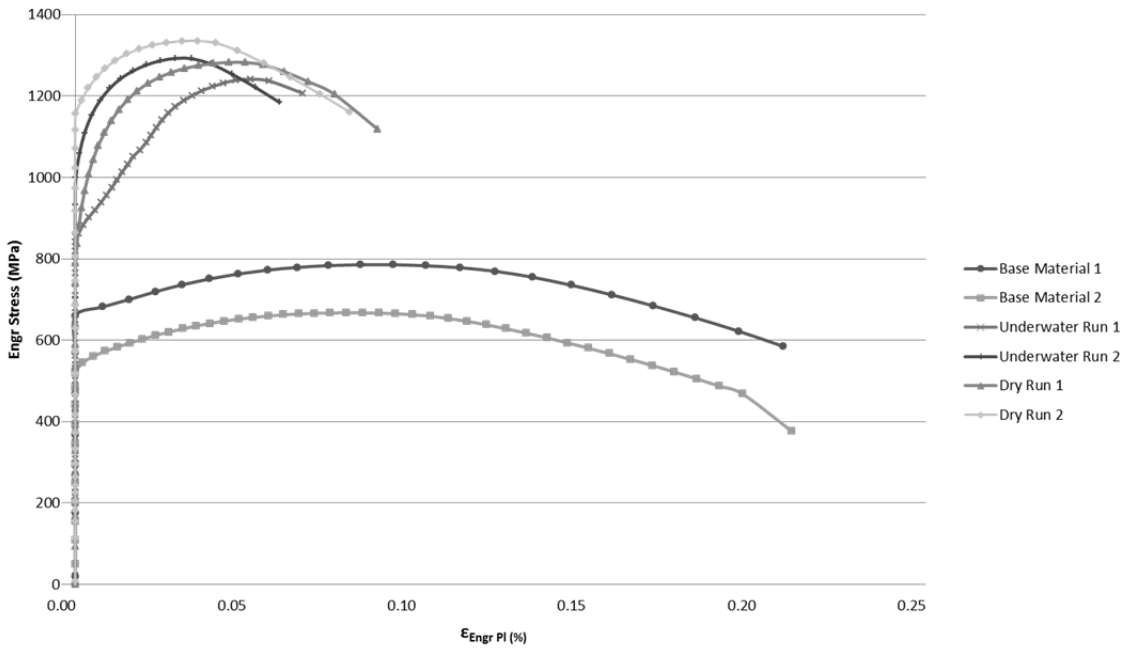

THIS PAGE INTENTIONALLY LEFT BLANK

LIST OF REFERENCES

[1] K. Masubuchi and D. C. Martin, "Mechanisms of cracking in HY-80 steel weldments," *Welding Journal,* vol. 41, pp. 375S–384S, 1962.

[2] J. H. Nixon, "Underwater repair technology," pp. 108, 2000. Amsterdam, Netherlands, Elsevier Science.

[3] LT N Overfield, "Feasibility of underwater friction stir welding of hardenable alloy steel," M.S. thesis, Naval Postgraduate School, September 2012.

[4] LT C Stewart, "Feasibility of underwater friction stir welding of HY-80 steel," M.S. thesis, Naval Postgraduate School, March 2011.

[5] W.M. Tomas. E.D. Nicholas, J.C. Needham, M.G. Murch, P. Temple-Smith, C.J. Dawes, "Fiction-stir butt welding," GB Patent No. 9125978.8, International patent application No. PCT/GB92/02203, 1991.

[6] R. S. Mishra, "Friction stir welding and processing," *Materials Science Engineering. R, Reports,* vol. 50, pp. 1, 2005.

[7] H. Fujii, "Friction stir welding of carbon steels," *Materials Science Engineering, Structural Materials,* vol. 429, pp. 50–57, 2006.

[8] T. Huang, "Microstructural evolution of DP980 steel during friction bit joining," *Metallurgical and Materials Transactions A Physical Metallurgy and Materials Science,* vol. 40, pp. 2994–3000, 2009.

[9] Y. C. Chen, "Evaluation of microstructure and mechanical properties in friction stir processed SKD61 tool steel," *Mater Charact,* vol. 60, pp. 1471–1475, 2009.

[10] Robert H. Todd, Dell K. Allen and Leo Alting, *Manufacturing Processes Reference Guide*. New York, NY: Industrial Press Inc., pp. 43–48, 1994.

[11] S. H. Aldajah, "Effect of friction stir processing on the tribological performance of high carbon steel," *Wear,* vol. 267, pp. 350–355, 2009.

[12] L. Cui, "Friction stir welding of a high carbon steel," *Scr. Mater.,* vol. 56, p. 637, 2007.

[13] A. Ozekcin, "A microstructural study of friction stir welded joints of carbon steels," *Int. J. Offshore Polar Eng.*, vol. 14, pp. 284, 2004.

[14] Y. D. Chung, H. Fujii, R. Ueji, and N. Tsuji, “Friction stir welding of high carbon steel with excellent toughness and ductility,” *Scr. Mater.*, vol. 63, pp. 223–226, 7, 2010.

[15] K. M. Richmond. (2010). RE: Assistance needed on welding questions. *E-mail correspondence from branch head for Code 250 - Submarine Structural, Puget Sound Naval Shipyard.*

[16] Military Specification, “MIL-S-16216K(SH),” pp. 4, 1987.

[17] Military Specification, “MIL-E-23765/2E,” pp. 10, 1994.

[18] Military Specification, “MIL-STD-248D,” 1997.

[19] I. Maroef, “Hydrogen trapping in ferritic steel weld metal,” *International Materials Reviews,* vol. 47, pp. 191–223, 2002.

[20] T. J. Lienert, “Friction stir welding studies on mild steel,” *Welding Journal*, vol. 82, pp. 1–9, 2003.

[21] K. Uehara, H. Takeshita, and H. Kotaka, “Hydrogen gas generation in the wet cutting of aluminum and its alloys.” *Journal of Materials Processing Technology*, vol. 127, pp. 174–177, 2002.

[22] Marine structural steel data bank; Ship structure committee, SSC-352, 1991.

[23] G. Kruass, *Principles of Heat Treatment of Steel*. Novelty, OH, American Society for Metals, pp. 129, 1980.

INITIAL DISTRIBUTION LIST

1. Defense Technical Information Center
   Ft. Belvoir, Virginia

2. Dudley Knox Library
   Naval Postgraduate School
   Monterey, California